PROJECTION HYDROCLIMATIQUE DE LA TENEUR EN EAU DES SOLS ET DES FAIBLES DÉBITS EN MILIEU FORESTIER

François Anctil

Janvier 2020

Ce projet est financé par le gouvernement du Québec et répond aux objectifs du Plan pour une économie verte 2030.

Table des matières

1. Introduction

Le 5e rapport du groupe d'experts intergouvernemental sur l'évolution du climat (GIEC, 2014) anticipe une perturbation accrue du climat mondial au cours des prochaines décennies. Au Québec, les changements climatiques se traduiront par une augmentation des températures et une intensification des précipitations (Ouranos, 2015), modifiant conséquemment l'évolution du régime hydrique. À l'horizon 2050, l'Atlas hydroclimatique du Québec méridional (MELCC, 2018) prévoit notamment une intensification très probable des épisodes d'étiage au cours de la période estivale, accentuant la vulnérabilité future des approvisionnements municipaux, industriels et agricoles. L'intensification projetée des étiages exercera également une pression sur la qualité de l'eau, la santé humaine, la croissance des végétaux et le maintien de la biodiversité (Abderregg *et al.* 2012, Aldous *et al.* 2011, Delpla *et al.* 2009). Quantifier l'impact des changements climatiques sur le régime hydrique permet la conception et la mise en œuvre de stratégies d'adaptation visant à minimiser la vulnérabilité future des usages de l'eau. Les analyses de l'impact des changements climatiques sur le régime hydrique s'appuient généralement sur le déploiement d'une chaîne de modélisation dite « hydroclimatique ». Cette dernière traduit le signal de changement inscrit dans les projections climatiques du GIEC à l'aide de modèles hydrologiques mis en place et calibrés dans le but de reproduire les processus hydrologiques à l'échelle du bassin versant.

2. Contexte / objectifs

Il est attendu que les changements climatiques accentuent les épisodes de faible débit et induisent une réduction importante de la réserve en eau utile des sols, affectant la production de la biomasse en milieu forestier. Les approches de modélisation généralement utilisées pour produire les projections hydroclimatiques sont affectées par des limitations méthodologiques importantes qui nuisent à une représentation adéquate des processus en conditions de stress hydrique. Les représentations simplifiées de l'évapotranspiration et des processus hydrodynamiques dans les couches superficielles de sol sont largement questionnées quant à leur capacité à maintenir une représentation adéquate des processus lorsque soumises à des conditions climatiques changeantes. Ces limitations sont exacerbées par la faible disponibilité de certaines observations météorologiques ainsi que d'une information pédologique détaillée, et ce, plus particulièrement en milieu forestier. L'objectif principal de ce projet consiste donc à produire des projections hydroclimatiques en renforçant la représentation de l'évapotranspiration et des processus hydrodynamiques dans les couches superficielles de sol pour un ensemble de bassins versants forestiers du Québec méridional.

3. Cadre théorique / compte-rendu de la revue de la littérature

Dans sa forme la plus conventionnelle, une projection hydrologique est construite en trois principales étapes (Madsen *et al.* 2014). Une simulation climatique est d'abord statistiquement post-traitée. Un modèle hydrologique est ensuite calibré à partir d'observations météorologiques et hydrométriques. La projection hydrologique est finalement construite en forçant le modèle hydrologique calibré avec la simulation climatique post-traitée. La Figure 1 présente en détail les étapes menant à la production d'une projection hydrologique à partir d'une configuration conventionnelle de la chaîne de modélisation hydroclimatique. Cette configuration s'avère dépendante des observations météorologiques disponibles parce qu'elle en fait un usage double, c'est-à-dire à la fois pour le post-traitement des variables climatiques simulées et le calage du modèle hydrologique (traits pointillés). La grande majorité des chaines de modélisation hydroclimatique documentées dans la littérature se limite

donc au traitement de la précipitation et de la température de l'air (Rössler *et al.* 2019, Olmos-Giménez *et al*. 2018, Tramblay *et al.* 2014) et conséquemment, à l'emploi de modèles hydrologiques configurés selon des représentations empiriques des processus. La configuration conventionnelle de la chaîne de modélisation hydroclimatique présente également la spécificité que le modèle hydrologique est calibré en étant forcé par la séquence historique des événements hydroclimatiques alors que la projection hydrologique (produite par le modèle calibré) est alimentée par la séquence d'événements simulée par le modèle climatique.

L'intégration des champs humidité de l'air, rayonnement solaire et vitesse du vent à la chaîne de modélisation hydroclimatique est nécessaire à une représentation davantage physique des processus hydrologiques. Cette pratique marginale demeure limitée à l'évaluation de l'évapotranspiration (Willkofer *et al.* 2018) ou bien à l'évolution du couvert nival (Sen Gupta et Tarboton 2016), pour les (rares) régions où de telles observations sont disponibles. Les réanalyses climatiques (Jones *et al.* 2017) sont de plus en plus utilisées pour simuler des débits en rivière (Essou *et al.* 2016, Fuka *et al.* 2014, Lauri *et al.* 2014, Haddeland *et al.* 2012), palliant ainsi le manque d'observations météorologiques nécessaires au forçage des modèles hydrologiques. Les réanalyses ne sont en contrepartie que très rarement utilisées pour le post-traitement statistique de simulations climatiques, ces dernières étant affectées par des biais et des disparités d'échelles relatives aux observations recueillies localement (Khedhaouiria *et al.* 2018, Grenier 2018, Diaconescu *et al.* 2017).

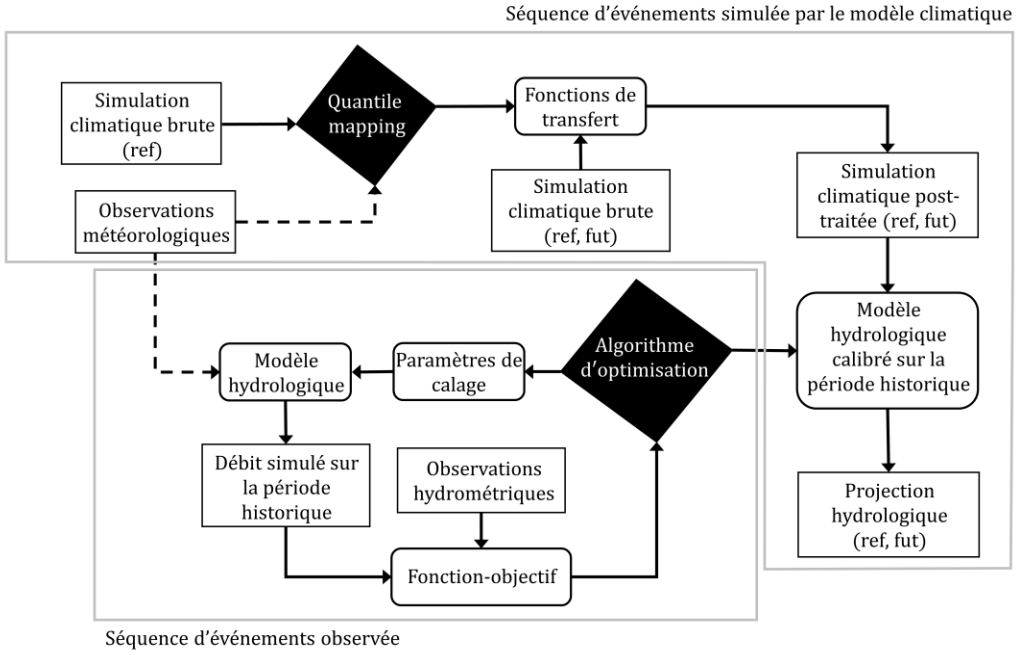

Figure 1. Configuration conventionnelle de la chaîne de modélisation hydroclimatique.

4. Méthodologie / données

La Figure 2 décrit en détail une configuration alternative de la chaîne de modélisation hydroclimatique contournant la problématique de la rareté de certaines observations météorologiques. Contrairement à la configuration conventionnelle, les fonctions de transfert nécessaires au post-traitement statistique des variables climatiques simulées sont calibrées de façon concomitante aux paramètres du modèle hydrologique. L'algorithme d'optimisation identifie d'abord une série de valeurs initiales aléatoires définissant les quantiles pour chaque fonction de transfert. Ces dernières sont ensuite appliquées aux variables climatiques simulées sur la période de référence. Le modèle hydrologique, également affecté d'un jeu aléatoire de valeurs paramétriques, est alimenté par la simulation climatique post-traitée sur la période de référence. Un critère d'erreur est ensuite évalué à partir de la projection hydrologique résultante et les débits observés disponibles. Les séquences d'événements ne coïncidant pas entre la projection hydrologique et les observations hydrométriques (voir Figure 1), le critère d'erreur doit intentionnellement ignorer le terme de corrélation entre les deux séries. Un tel critère d'erreur est nommé « fonction-objectif asynchrone ». Minimisant ce critère d'erreur, l'algorithme d'optimisation converge itérativement vers une solution optimale pour les fonctions de transfert et les paramètres du modèle hydrologique. Une fois l'optimisation complétée, la construction de la projection hydrologique (traits pointillés) est conceptuellement équivalente à celle de la configuration conventionnelle, c'est-à-dire que le modèle hydrologique calibré est alimenté avec les séries climatiques post-traitées. La configuration alternative proposée présente la caractéristique principale de ne faire appel à aucune observation météorologique, ni pour opérer le post-traitement statistique des variables climatiques simulées ni pour calibrer le modèle hydrologique.

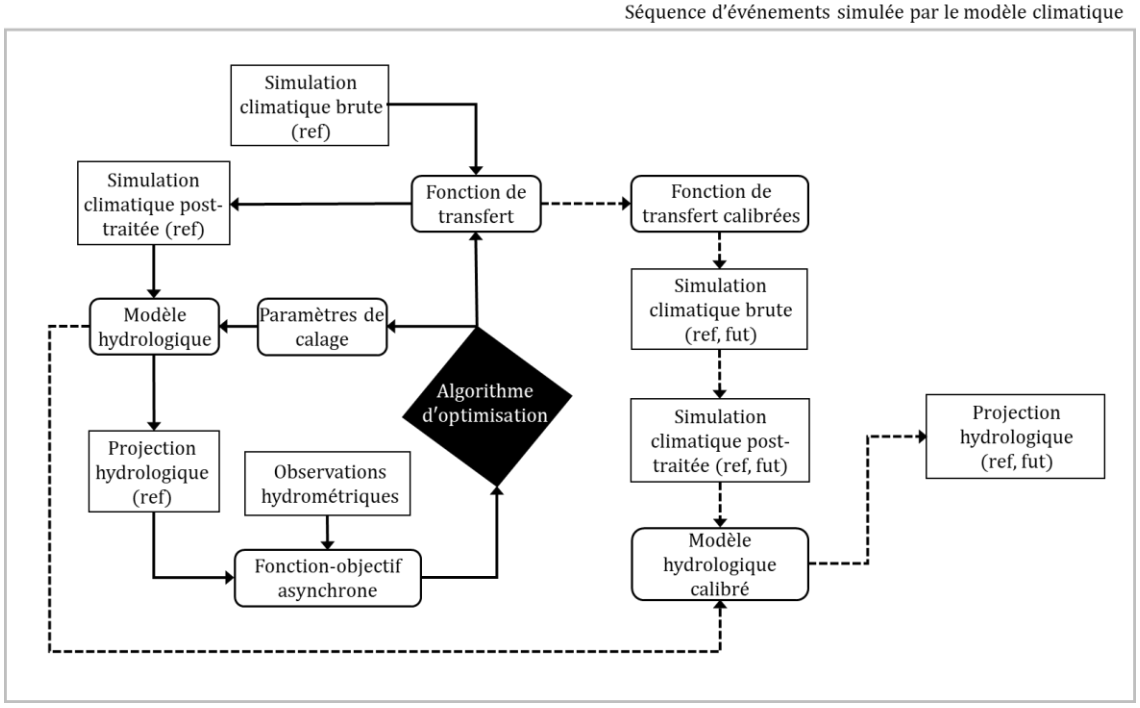

Figure 2. Configuration alternative de la chaîne de modélisation hydroclimatique.

Une chaîne complète de modélisation hydroclimatique intégrant les champs humidité de l'air, rayonnement solaire et vitesse du vent est mise en place sur un bassin versant forestier de la vallée du Saint-Laurent selon les configurations conventionnelle et alternative. L'intégration des champs humidité de l'air, rayonnement solaire et vitesse du vent à la chaîne de modélisation permet de construire une chronique d'évapotranspiration à partir de la formulation de Penman-Montheith (Allen *et al.* 1998). Les projections hydrologiques sont construites à partir des simulations climatiques issues du projet de mise à l'échelle dynamique régionale CRCM5-LE (Leduc *et al.* 2019). Afin de pallier le manque d'observation des champs humidité de l'air, rayonnement solaire et vitesse du vent, la configuration conventionnelle emploie les champs correspondants simulés par quatre réanalyses largement documentées dans la littérature soit, CFSR (Saha *et al.* 2014), MERRA-2 (Gelaro *et al.* 2017), ERA-Interim (Dee *et al.* 2011) et JRA-55 (Kobayashi *et al.* 2015). Le modèle hydrologique distribué à base physique WaSiM-ETH (Schulla 2019) est mis en place à partir des données distribuées décrivant la physiographie du bassin : topographie, réseau hydrographique, occupation du territoire et texture de sol. Le choix d'un modèle hydrologique à base physique est motivé par le souhait de réduire autant que possible le processus de compensation paramétrique pouvant affecter le calage des fonctions de transfert. En comparaison à des modèles hydrologiques plus conceptuels, WaSiM-ETH propose notamment une représentation davantage sophistiquée des écoulements et de l'évolution de la teneur en l'eau du sol. Le modèle WaSiM-ETH est calibré avec un nombre restreint de paramètres à l'aide de l'algorithme d'optimisation multi-critères Pareto archived dynamically dimensioned search (PA-DDS, Asadzadeh et Tolson 2012). Cet algorithme, couramment utilisé dans la pratique, est conçu pour converger rapidement vers des solutions localement optimales (même avec un nombre limité d'itérations), facilitant ainsi le calage de modèles hydrologiques distribués exigeants en temps calcul.

5. Résultats

Un premier manuscrit (Ricard et Anctil 2019, publié dans la revue *Water* en juin 2019, voir annexe 1) vise à démontrer l'applicabilité de la formulation de Penman-Montheith alimentée par les champs humidité de l'air, rayonnement solaire et vitesse du vent issus de réanalyses. Pour ce faire, le modèle hydrologique WaSiM-ETH a été mis en place et calibré sur six bassins versants de la vallée du Saint-Laurent présentant un régime hydrique naturel et une occupation à dominance forestière. Les résultats obtenus révèlent que la nature des biais affectant les champs simulés par réanalyses est spécifique à la réanalyse ainsi qu'au champ simulé. La qualité de la réponse hydrologique simulée par le modèle calibré ne semble pas liée à capacité de la réanalyse à simuler adéquatement les forçages climatiques. Cette observation suggère que le calage du modèle tend à identifier des solutions paramétriques optimales compensant les biais empreints dans les séries climatiques simulées par les réanalyses. Une approche de correction de biais basée sur la calibration de facteurs saisonniers a mené à une amélioration modérée de la réponse hydrologique résultante, spécifique au biais hydrologique lors de la période pluviale (de juin à novembre).

Un second manuscrit (Ricard *et al.* 2019, publié dans la revue *Water* en septembre 2019, voir annexe 2) met d'abord en contexte la pratique usuelle par laquelle les projections hydrologiques sont construites. Il identifie également les limites conceptuelles liées au déploiement d'une chaîne de modélisation hydroclimatique selon une configuration conventionnelle. Il définit ensuite la notion de fonction-objectif asynchrone et propose une configuration alternative de la chaîne de modélisation visant à corriger l'usage redondant des observations météorologiques (Figure 1). Cette configuration alternative est mise en place sur le bassin versant de la rivière Du Loup (022507) à partir des simulations climatiques

CRCM5-LE et du modèle hydrologique WaSiM-ETH et comparée à une configuration conventionnelle. Cinq fonctions-objectifs asynchrones de natures variées sont imaginées et testées à titre exploratoire. Les plus performantes démontrent un comportement en validation similaire à celui de la métrique Kling-Gupta-Efficiency (KGE, Gupta *et al.* 2009) sur la période historique observée, à l'exception d'une légère dégradation de la variance et de la corrélation entre les séries hydrologiques simulées et observées sur la période estivale. Les projections hydrologiques simulées sur la période de référence à partir de la configuration alternative démontrent un comportement davantage cohérent que celles produites à partir de la configuration conventionnelle.

Un troisième manuscrit (à soumettre) porte sur l'intégration des champs humidité de l'air, rayonnement solaire et vitesse du vent à la chaîne de modélisation hydroclimatique dans le but de produire des projections hydrologiques à partir de la formulation de Penman-Montheith. Une configuration conventionnelle substituant les observations météorologiques par des réanalyses ainsi qu'une configuration alternative ont été mise en place sur le bassin versant de la rivière Du Loup. La configuration alternative intègre ici le calage des fonctions de transfert appliquées aux variables climatiques simulées ainsi que des paramètres du modèle hydrologique. Les résultats obtenus confirment que les projections hydrologiques simulées sur la période de référence à partir de la configuration alternative démontrent un comportement davantage cohérent que celles produites à partir de la configuration conventionnelle. Ceci s'explique par le fait que les biais inscrits dans les réanalyses altèrent la nature du signal de changement identifié par l'analyse des projections hydrologiques, affectant les simulations climatiques post-traitées ainsi que l'identification des paramètres optimaux lors du calage du modèle hydrologique.

Un quatrième manuscrit (en cours de production) cherche à évaluer la valeur ajoutée des propriétés hydrodynamiques des couches superficielles de sol inférées par la DRF-MFFP par rapport aux données produites d'autres produits plus couramment utilisés en modélisation hydrologique distribuée. La réponse hydrologique simulée par le modèle hydrologique WaSiM-ETH simulée sera évaluée sur cinq bassins versants forestiers du Québec. Les processus hydrologiques intermédiaires (évapotranspiration, couvert de neige et teneur en eau dans le sol) seront également validés avec les observations recueillies sur le site expérimental du BEREV (Isabelle, 2018).

6. Analyse et discussion

Les configurations conventionnelles exigent des séries climatiques suffisamment longues et en densité suffisante afin d'opérer le post-traitement statistique des simulations et le calage du modèle hydrologique. La configuration alternative proposée suggère le calage des fonctions de transfert du post-traitement statistique conjointement au calage des paramètres du modèle hydrologique. Cette configuration s'appuie sur l'hypothèse que les fluctuations de débits observés à l'exutoire d'un bassin versant constituent un proxy fonctionnel du forçage climatique correspondant. Cette hypothèse constitue évidemment une simplification réductrice du point de vue de la représentation des processus climatiques. Les travaux conduits dans le cadre de ce projet tendent à démontrer qu'elle peut s'avérer utile et justifiée dans l'optique de la construction de projections hydrologiques à partir d'une modélisation reposant davantage sur la description physique des processus à l'échelle du bassin versant et ce, dans un contexte de rareté de certaines observations météorologiques.

L'analyse des résultats présentés en annexe supportent les conclusions suivantes :

i. Les champs humidité, rayonnement et vent simulés par les réanalyses sont biaisés relativement aux observations disponibles. Les projections hydrologiques construites selon une configuration conventionnelle s'avèrent sensibles aux biais inscrits dans les réanalyses.
ii. Une fonction-objectif asynchrone minimisant l'erreur sur l'hydrogramme interannuel moyen tend produire une réponse hydrologique équivalente à la métrique KGE. L'ajout de critères liés à la variance des séries améliore la représentation des valeurs hydrologiques extrêmes.
iii. La configuration alternative proposée de la chaîne de modélisation hydroclimatique produit des projections hydrologiques davantage représentative du régime hydrologique observé par rapport à celles issues de configurations conventionnelles employant des réanalyses climatiques biaisées.
iv. La projection de l'évapotranspiration, de la teneur en eau dans le sol et des faibles débits estivaux est sensible au choix de la formulation d'évapotranspiration.

De façon plus large, les travaux conduits dans le cadre de ce projet s'inscrivent dans la perspective qu'une modélisation à base physique induit une valeur ajoutée relative à la confiance imputée aux projections hydrologiques. Pour renforcer les conclusions présentées ci-dessus, de futurs travaux devront s'attarder à les généraliser à de multiples ensembles climatiques, de multiples modèles, de multiples formulations d'évapotranspiration et davantage de sites. Le développement d'une stratégie de calage adaptée à la configuration alternative proposée permettrait d'accroître le nombre de critères d'optimisation composant les fonctions-objectifs asynchrones et ainsi potentiellement améliorer la qualité et la robustesse des projections hydrologiques construites. Intégrer des variables intermédiaires (évapotranspiration, neige au sol, teneur en eau dans le sol) au calcul des fonctions-objectifs asynchrones renforcerait aussi la robustesse des projections hydrologiques. Il serait également pertinent d'évaluer la capacité de la configuration alternative à post-traiter les précipitations, températures ou rayonnement d'ondes longues simulés par les modèles climatiques.

7. Conclusion et recommandations

Ce projet propose une configuration alternative de la chaîne de modélisation hydroclimatique permettant la construction de projections hydroclimatiques en milieu forestier à partir de la formulation de Penman-Montheith malgré l'absence des certaines observations météorologiques nécessaires au forçage de cette dernière. Les retombées ouvrent finalement la porte au déploiement d'une modélisation hydroclimatique à base physique en milieu forestier où certaines observations météorologiques sont rares. En intégrant les champs humidité de l'air, rayonnement solaire et vitesse du vent, il est possible d'entrevoir un élargissement de la portée de la chaîne de modélisation hydroclimatique, traduisant localement l'impact projeté des changements climatiques sur d'autres variables telles que la température de l'eau, la formation de glace en rivière et la croissance des végétaux.

8. Références

Aldous, A., Fitzsimons, J., Richter, B., and Bach, L., 2011. Droughts, floods and freshwater ecosystems: evaluating climate change impacts and developing adaptation strategies. Marine and Freshwater Research, 62(3), 223-231.

Allen, R.G., Pereira, L.S., Raes, D., and Smith, S., 1998. Crop Evapotranspiration - Guidelines for Computing Crop Water Requirements; Irrigation and Drainage Paper 56. FAO, Rome, Italy, 1-15.

Anderegg, W.R.L., Anderegg, L.D.L., Sherman, C. and Karp, D.S., 2012. Effects of widespread drought-induced aspen mortality on understory plants. Conservation Biology, 26(6), 1082-1090.

Asadzadeh, M. and Tolson, B., 2012. Hybrid Pareto archived dynamically dimensioned search for multi-objective combinatorial optimization: application to water distribution network design. Journal of Hydroinformatics, 14(1), 192-205.

Dee, D. P., *et al.*, 2011. The ERA-Interim Reanalysis: Configuration and Performance of the Data Assimilation System. Quarterly Journal of the Royal Meteorological Society, 137(656), 553–597.

Delpla, I., Jung, A.V., Baures, E., Clement, M., and Thomas, O., 2009. Impacts of climate change on surface water quality in relation to drinking water production. Environment International, 35(8), 1225-1233.

Diaconescu, E. P., Mailhot, A., Brown, R., and Chaumont, D., 2017. Evaluation of CORDEX-Arctic daily precipitation and temperature-based climate indices over Canadian Arctic land areas. Climate Dynamics, 50(5-6), 2061–2085.

Essou, G. R. C., Sabarly, F., Lucas-Picher, P. Brissette, F., and Poulin, A., 2016. Can Precipitation and Temperature from Meteorological Reanalyses Be Used for Hydrological Modeling? Journal of Hydrometeorology, 17(7), 1929–1950.

Fuka, D. R., Walter, M. T., MacAlister, C., Degaetano, A. T., Steenhuis, T.S., and Easton, Z. M., 2014. Using the Climate Forecast System Reanalysis as Weather Input Data for Watershed Models. Hydrological Processes, 28(22), 5613–5623.

Gelaro, R., *et al.*, 2017. The Modern-Era Retrospective Analysis for Research and Applications, Version 2 (MERRA-2). Journal of Climate, 30(14), 5419–5454.

Grenier, P., 2018. Two types of physical inconsistency to avoid with univariate quantile mapping: A case study over North America concerning relative humidity and its parent variables. Journal of Applied Meteorology and Climatology, 57(2), 347-364.

Gupta, H.V., Kling, H., Yilmaz, K.K., and Martinez, G.F., 2009. Decomposition of the mean squared error and nse performance criteria: implications for improving hydrological modelling. Journal of Hydrology, 377, 80–91.

Haddeland, I., Heinke, J., Voss, F., Eisner, S., Chen, C., Hagemann, S., and Ludwig, F., 2012. Effects of climate model radiation, humidity and wind estimates on hydrological simulations. Hydrology and Earth System Sciences, 16(2), 305-318.

IPCC, 2014: Climate Change 2014: Synthesis Report. Contribution of Working Groups I, II and III to the Fifth Assessment Report of the Intergovernmental Panel on Climate Change. IPCC, Geneva, Switzerland, 151 pp.

Isabelle, P. E., Nadeau, D. F., Asselin, M. H., Harvey, R., Musselmane, K. N., Rousseau A. N., and Anctil F., 2018. Solar radiation transmittance of a boreal balsam fir canopy: Spatiotemporal variability and impacts on growing season hydrology. Agricultural and Forest Meteorology, 263, 1-14.

Jones, P. D., Harpham, C., Troccoli, A., Gschwind, B., Ranchin, T., Wald, L., Goodess, C. M., and Dorling, S., 2017. Using ERA-Interim Reanalysis for Creating Datasets of Energy-Relevant Climate Variables. Earth System Science Data, 9, 471-495.

Khedhaouiria, D., Mailhot, A., and Favre, A. C. 2018. Stochastic Post-Processing of CFSR Daily Precipitation across Canada. Atmosphere Ocean, 56(2), 104-116.

Kobayashi, S., Ota, Y., Harada, Y., Ebita, A., Moriya, M., Onoda, H., Onogi, K., Kamahori, H., Kobayashi, C., Endo, H., Miyaoka, K., and Takahashi, K., 2015. The JRA-55 Reanalysis: General Specifications and Basic Characteristics. Journal of the Meteorological Society of Japan, 93(1), 5-48.

Lauri, H., Räsänen, T.A., and Kummu, M., 2014. Using reanalysis and remotely sensed temperature and precipitation data for hydrological modeling in monsoon climate: Mekong river case study. Journal of Hydrometeorology, 15, 1532-1545.

Leduc, M., Mailhot, A., Frigon, A., Martel, J. L., Ludwig, R., Brietzke, G.B., Giguère, M., Brissette, F., Turcotte, R., Braun, M., and Scinocca, J., 2019. The ClimEx Project: A 50-Member Ensemble of Climate Change Projections at 12-km Resolution over Europe and Northeastern North America with the Canadian Regional Climate Model (CRCM5). Journal of Applied Meteorology and Climatology, 58(4), 663-693.

Madsen, H., Lawrence, D., Lang, M., Martinkova, M., and Kjeldsen, T. R., 2014. Review of trend analysis and climate change projections of extreme precipitation and floods in Europe. Journal of Hydrology, 519, 3634–3650.

Ministère de l'Environnement et de la Lutte contre les changements climatiques (MELCC). Atlas hydroclimatique du Québec méridional. Édition 2018. Québec, Québec. http://www.cehq.gouv.qc.ca/atlas-hydroclimatique (consulté le 08 juillet 2019).

Olmos Giménez, P., García-Galiano, S. G., Giraldo-Osorio, J. D, 2018. Improvement of hydroclimatic projections over southeast Spain by applying a novel RCM ensemble approach. Water, 10(52), 1-19.

Ouranos (2015). Vers l'adaptation. Synthèse des connaissances sur les changements climatiques au Québec. Partie 1 : Évolution climatique au Québec. Édition 2015. Montréal, Québec, Ouranos, 114 p.

Ricard, S. and Anctil, F., 2019. Forcing the Penman-Montheith Formulation with Humidity, Radiation, and Wind Speed Taken from Reanalyses, for Hydrologic Modeling. Water, 11(6), 1-15.

Ricard, S., Sylvain, J.D. and Anctil, F., 2019. Exploring an Alternative Configuration of the Hydroclimatic Modeling Chain, Based on the Notion of Asynchronous Objective Functions. Water, 11(10), 1-18.

Rössler, O., Kotlarski, S. Fischer, A. M., Keller, D., Liniger, M., and Weingartner, R., 2019. Evaluating the added value of the new Swiss climate scenarios for hydrology: An example from the Thur catchment. Climate Services, 13, 1-13.

Saha, S., *et al.*, 2014. The NCEP Climate Forecast System Version 2. Journal of Climate, 27(6), 2185–2208.

Schulla, J., 2019. Model Description WaSiM. www.wasim.ch (consulté le 08 juillet 2019).

Sen Gupta, A. and Tarboton, D.G., 2016. A Tool for Downscaling weather data from large-grid reanalysis products to finer spatial scales for distributed hydrological applications. Environmental Modelling and Software, 84, 50-69.

Tramblay, Y., Amoussou, E., Dorigo, W., and Mahé, G., 2014. Flood risk under future climate in data sparse regions: Linking extreme value models and flood generating processes. Journal of Hydrology, 519, 549-558.

Willkofer, F., Schmid, F.J., Komischke, H., Korck, J., Braun, M., and Ludwig, R., 2018. The impact of bias correcting regional climate model results on hydrological indicators for Bavarian catchments. Journal of Hydrology: Regional Studies. 19, 25-41.

Annexe 1 : Article publié dans la revue *Water* en juin 2019

water

MDPI

Article

Forcing the Penman-Montheith Formulation with Humidity, Radiation, and Wind Speed Taken from Reanalyses, for Hydrologic Modeling

Simon Ricard * and François Anctil

Department of Civil and Water Engineering, Laval University, Québec, QC G1V 0A6, Canada; Francois.Anctil@gci.ulaval.ca

* Correspondence: simon.ricard.1@ulaval.ca

Received: 8 April 2019; Accepted: 3 June 2019; Published: 11 June 2019

Abstract: The Penman-Monteith reference evapotranspiration (ET_0) formulation was forced with humidity, radiation, and wind speed (HRW) fields simulated by four reanalyses in order to simulate hydrologic processes over six mid-sized nivo-pluvial watersheds in southern Quebec, Canada. The resulting simulated hydrologic response is comparable to an empirical ET_0 formulation based exclusively on air temperature. However, Penman-Montheith provides a sounder representation of the existing relations between evapotranspiration fluctuations and climate drivers. Correcting HRW fields significantly improves the hydrologic bias over the pluvial period (June to November). The latter did not translate into an increase of the hydrologic performance according to the Kling-Gupta Efficiency (KGE) metric. The suggested approach allows for the implementation of physically-based ET_0 formulations where HRW observations are insufficient for the calibration and validation of hydrologic models and a potential reinforcement of the confidence affecting the projection of low flow regimes and water availability.

Keywords: hydrology; modeling; evapotranspiration; reanalysis; Penman-Monteith; humidity; radiation; wind speed

1. Introduction

Evapotranspiration (ET) is a key process in the representation of hydroclimatic flows and budgets. It is defined as the transfer of water vapor to the atmosphere from a surface or through plant stomata. Four main meteorological drivers determine ET fluctuations: air temperature, net radiation, humidity, and wind speed. The ET fluxes are rarely measured, and estimation approaches are affected by large uncertainties. In hydrologic modeling, ET is typically treated as a component of the water balance at the scale of a watershed. Reference evapotranspiration (ET_0) is estimated from available climate variables and leads to ET when considering soil water and vegetation cover conditions. Hydrologic models are sensitive to the selection of a given ET_0 formulation [1] since it influences their parametric configuration and consequently the yearlong hydrologic regime, including streamflow, soil water content, and snow water equivalent. This influence persists in projections forced under different radiative forcing scenarios [2]. The arguments for deciding upon which ET_0 formulation to use are not widely consensual [3–5]. On the one hand, empirical ET_0 formulations, based exclusively on air temperature, are widely used in hydrology because they are simple to evaluate and perform well in the scope of simulating river flows [6]. On the other hand, formulations integrating to various degrees air humidity, radiation, and wind speed (hereinafter referred to as HRW fields) remains limited by the amount, quality, and representativeness of the available observations.

Forcing hydrologic models with fields simulated by climate reanalyses is becoming progressively common in order to overcome the low density of meteorological observations. Works described in the

recent literature [7–13] demonstrate the capacity of reanalyses to provide consistent hydrologic responses. They may even surpass observations in some instances [9]. The quality of the resulting hydrologic response seems however strongly related to the reanalysis ability to simulate precipitation [8,14]. Downscaling simulated precipitation and correcting bias may substantially improve simulated flows, especially for watersheds presenting complex topographic features [12]. Forcing hydrologic models with reanalyses is typically limited to the use of precipitation and temperature fields and, therefore, to empirical ET_0 formulations based exclusively on air temperature.

The ability of reanalyses to simulate HRW fields and their relevance to hydrologic modeling is much less documented [15–17]. The correspondence between ET_0 values from the Penman-Montheith (PM) formulation respectively forced by in situ observations and fields taken from a reanalysis have been demonstrated over China with the European Centre for Medium-Range Weather Forecasting (ECMWF) ERA-Interim reanalysis [18] and over the Iberian Peninsula with the National Center for Environmental Prediction/National Center for Atmospheric Research(NCEP/NCAR) reanalysis [19]. Huang et al. [20] combined surface radiation and temperature from the National Aeronautics and Space Administration–Clouds and the Earth's Radiant Energy System (NASA-CERES) and surface specific humidity from the NASA-Modern Era Retrospective-analysis for Research and Applications (MERRA) reanalysis to force the maximum-entropy-production (MEP) model of surface heat fluxes. Yao et al. [21] estimate ET_0 by forcing the PM formulation with a combination of the Global Energy and Water Cycle Experiment (GEWEX) Surface Radiation Budget dataset (SRB) and weather observations. The authors conclude that a PM-based approach provides consistent interannual trajectories relative to water budget estimates.

Sperna Weiland et al. [22] forced six ET_0 formulations on a global scale with the NCEP Climate Forecast System Reanalysis (CFSR) and CRU dataset (Climate Research Unit, University of East Anglia) and concluded that PM does not outperform simpler ET_0 formulations. They argued that their finding may be explained by the limited capacity of the source data, CRU and CFSR, to reproduce the atmospheric fields that forces the PM formulation. Jones et al. [23] demonstrated the benefit of correcting biases in ERA-Interim HRW fields. Sen Gupta and Tarboton [24] developed and applied a downscaling method for temperature, relative humidity, radiation and wind speed taken from MERRA reanalysis in order to simulate the snowpack at 173 sites across the United States. None of the above focused on the hydrologic response at the watershed scale. Essou et al. [25] combined precipitation and temperature observations with supplemental fields from ERA-Interim, CFSR, and MERRA reanalyses for hydrologic modeling. They compared the weighted-average of the meteorological sources and of the hydrologic response. They found that both methods improve the hydrologic response of a large number of watersheds spread across the United States and Canada. Lauri et al. [11] demonstrated the interest of combining temperature simulated by CFSR with precipitation observation for simulating the Mekong streamflow.

The work described in this study aims to answer the following question: are humidity, radiation, and wind speed (HRW fields), as simulated by reanalyses, functional surrogates to observations in providing a consistent, physically-based, simulated hydrologic response. The Penman-Montheith formulation is forced by a combination of interpolated temperature and precipitation observations and HRW fields taken from four state-of-the-art reanalyses. The resulting hydrologic responses (simulated streamflow and state variables, here focusing on evapotranspiration) are evaluated and compared to a temperature-based ET_0 formulation. The study also evaluates the impact of reanalyses biases on the simulated hydrologic response and explores a calibration-based (observation-free) correction of the forcing HRW fields.

The suggested approach allows a pragmatic solution to simulate hydrologic processes over a watershed using a more physically-based ET_0 formulation even where HRW observations are insufficient or absent. Without formally exploring this idea, Auerbach et al. [7] suggested exploiting the HRW fields from the CFSR reanalysis in order to simulate hydrologic processes on more mechanistic grounds. Considering the climate change-driven increase of the air temperature and modification of

the HRW fields, we believe the usage of a physically-based ET_0 formulation, even partially forced by reanalyses, supports the construction of more reliable streamflow projections at the catchment scale.

2. Domain, Data, and Methodology

2.1. Domain

The analysis is conducted over six intermediate-size catchments (512 to 761 km^2) located in the Province of Quebec, Canada, between latitudes 45° N and 48° N and longitudes −69° E and −75° E (Q1 to Q6, Figure 1). Monthly air temperature fluctuates from −13 °C (January) to 20 °C (July) and yearly precipitation, from 1000 mm to 1200 mm. Daily relative humidity remains somehow constant throughout summer and fall (~80%) but declines in April and May (~60%). Daily downwelling shortwave radiation (site R1) peaks in June (5500 W/m^2) and plummets in December (1000 W/m^2). Daily wind speed is fairly constant from November to March (up to 3 m/s) but lowers throughout summer (2 m/s). All sites are categorized as mixed nivo-pluvial hydrologic regime characterized by an important spring freshet and autumnal highs. Streamflow typically peaks in April when the snowpack melts. A second but lesser peak follows lower autumnal evapotranspiration and intensification of synoptic precipitations. Low flows dominate winter and are common in summer because of the accumulation of the snowfall and of maximum evapotranspiration, respectively. All basins are characterized by moderate slopes (4.1%–13.4%). Forest is the dominant land use (59%–83%) while sites Q3 and Q5 present a significant portion of agricultural and urbanized lands (32% and 35%, respectively). All flows are quite free from the upstream influence of the dam operations, with DOR values ("degree of regulation") not exceeding 8% for all basins [26].

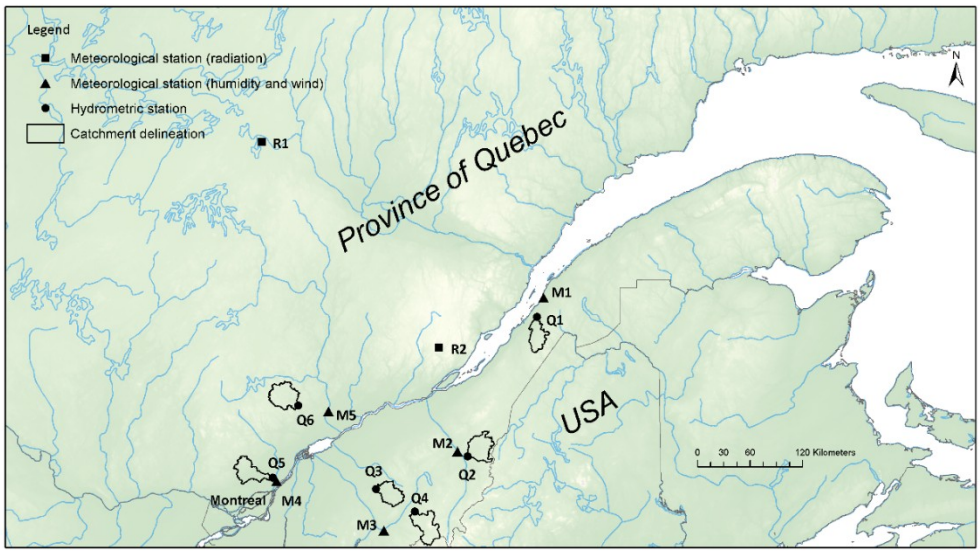

Figure 1. Location of the outlet of the six catchments (circles) and of the nearest meteorological stations (triangles and squares) from which humidity, radiation and wind speed observations are extracted.

2.2. Data

Daily hydrometric observations are provided by the Quebec hydrometric network and daily precipitation and temperature observations, from Quebec Climate Monitoring Program. Precipitation and temperature observations are interpolated by kriging on a 0.1-degree grid. Relative humidity and wind speed observations are extracted from the closest Environment and Climate Change Canada weather stations (sites M1 to M5, Figure 1, Table 1). The distance to the corresponding hydrometric station ranges from 6.4 to 49.2 km. Short wave radiation and latent heat flux observations are extracted respectively at Black Spruce/Jack Pine site (R1, 49.27° N and −74.04° E) and Forêt Montmorency (R2, 47.27° N and −71.12° E) experimental sites. R1 is located further north, the distance to sites Q1 to Q6

varies from 304 to 458 km. Data are available from 2005 to 2009 at site R1 and from 2016 to 2018 at site R2.

Table 1. Description of hydrometric stations.

Site	Latitude (°N)	Longitude (°E)	Area (km^2)	Forest Land Use (%)	Slope (%)	Corresponding Meteorological Station
Q1	47.6	−69.7	512	77	5.9	M1
Q2	46.2	−70.6	695	75	4.1	M2
Q3	45.8	−72.0	549	60	5.8	M3
Q4	45.6	−71.4	736	79	7.9	M3
Q5	45.9	−73.5	633	59	6.4	M4
Q6	46.6	−73.2	761	83	13.4	M5

Preprocessing is applied to the relative humidity, downwelling shortwave radiation, and wind speed (the HRW fields) taken from CFSR [27], MERRA-2 [28], ERA-Interim [29], and the Japanese 55-year atmospheric reanalysis (JRA-55 [30,31]) reanalyses. Experimenting numerous forcing data sets allows the evaluation of the sensitivity of the simulated hydrological response to reanalyses biases. Simulated HRW fields are combined to precipitation and temperature observations for two reasons. First, to circumvent the documented impact of large biases affecting precipitation taken from reanalyses on the simulated hydrological response (see Introduction). Second, precipitation and temperature observations are readily available at the regional scale to force hydrological models on numerous catchments, which is rarely the case for HRW fields. Reanalyses data units are harmonized and integrated into a daily time step. The average daily wind speed is the vector average of the North-South and East-West components. MERRA-2 and JRA-55 relative humidity values are calculated from the air and dew point temperatures using the following formulation:

$$RH = 100 \times 10^{m\left[\frac{T_{dw}}{T_{dw}+T_n} - \frac{T}{T+T_n}\right]} \quad (1)$$

where RH is the relative humidity (%), T_{dw}, dew point temperature (°C), T, air temperature (°C), m (–) and T_n (°C), empirical constants for specific temperature ranges.

2.3. Hydrologic Modeling Setup

Table 2 summarizes the hydrologic modeling setup designed for this study. The Richards-9.02.00 version of the physically-based distributed hydrologic model WaSim-ETH [32–34] is implemented over the six catchments described in Section 2.1. The river network is generated from a burned 50-m resolution digital elevation model, resampled to 500 m and manually corrected for each catchment. Land use is extracted from various sources provided by local agencies. Reference evapotranspiration (ET_0) is evaluated on the Penman-Montheith (PM) formulation [35]:

$$\lambda E = \frac{\Delta(R_n - G) + \rho_a c_p\left(\frac{e_s - e_a}{r_a}\right)}{\Delta + \gamma\left(1 + \frac{r_s}{r_a}\right)} \quad (2)$$

where λ is the latent vaporization heat (KJ·Kg^{-1}), E, the latent heat flux (Kg·m^{-2}), R_n, net radiation (Wh·m^{-2}), G, soil heat flux (Wh·m^{-2}), $(e_s - e_a)$, vapour pressure deficit of the air (hPa), ρ_a, $m$ean air density at constant pressure (Kg·m^{-3}), c_p, specific heat of the air (KJ·(Kg·K)$^{-1}$), Δ, tangent of the saturated vapor pressure curve (hPa·K^{-1}), γ, psychrometric constant (hPa·K^{-1}), r_s and r_a, surface and aerodynamic resistances (s·m^{-1}).

The PM formulation is forced by observed temperature and humidity, radiation, and wind speed time series taken from reanalyses (Section 2.2) and compared in Sections 3.2 and 3.3 to the Hamon empirical temperature-based formulation:

$$E_0 = 0.1651 \times f_i \times \frac{h_d}{12} \times \frac{216.6 \times e_s}{T + 273.3} \quad (3)$$

where f_i is an empirical correction factor (-), h_d, day length (h), and e_s, the saturation vapor pressure at temperature T (hPa).

Solid precipitations are corrected according to Equation (4) using a threshold temperature:

$$P_{cor} = a_s \times P \qquad T < T_{tr} \quad (4)$$

where P_{cor} is the corrected solid precipitation (mm), a_s, a correction parameter (-), and T_{tr}, a threshold temperature for snow/rain transition (°C).

Snowmelt is simulated using a temperature-index degree-day method:

$$M = c_0(T - T_m) \times \frac{\Delta t}{24} \quad (5)$$

where M is the melting rate (mm·day^{-1}), c_0, a temperature dependent melt factor (mm·°C^{-1}·day^{-1}), T_m, the temperature limit for snow melt (°C), and Δt, the simulation time step (24 h).

Vertical fluxes within the unsaturated zone are based on the Richards equation applied to a 10-m deep column composed of 30 numeric layers. An empirical fraction determines the portion of snow melt taken as surface runoff, considering sufficient snow cover on the ground:

$$Q_s = Q_{snw} \times QD_{snw} \quad (6)$$

where Q_s is the surface runoff (mm), Q_{snw}, snow melt (mm), and QD_{snw}, a fraction of Q_s on Q_{snw} (-).

Soil textures (percentages of clay, silt, and sand) originate from Shangguan et al. [36], while transient soil hydraulic properties follow Van Genuchten equations. Interflow is generated at soil layer boundaries considering slope and hydraulic conductivity:

$$Q_h = k_s(\theta_m) \times \Delta z \times d_r \tan(\beta) \quad (7)$$

where Q_h is the interflow (ms^{-1}), k_s, the saturated hydraulic conductivity (ms^{-1}), θ_m, the soil water content in layer m (-), Δz, layer thickness (m), d_r, a scaling parameter to consider river density (m^{-1}), and β, the local slope angle (°).

Both surface runoff and interflow are delayed using recession constants:

$$Q_{s,i} = Q_{s,i-1} \times e^{-\Delta t/k_s} + Q_s \times \left(1 - e^{-\Delta t/k_s}\right) \quad (8)$$

$$Q_{h,i} = Q_{h,i-1} \times e^{-\Delta t/k_h} + Q_h \times \left(1 - e^{-\Delta t/k_h}\right) \quad (9)$$

where $Q_{s,i}$ and $Q_{h,i}$ are delayed surface runoff and interflow at time step i (mm), Q_s and Q_h, surface runoff and interflow at time step i (mm), Δt, time step (h), k_s and k_h, recession constants (h).

Table 2 also identifies WaSim-ETH's free-parameters and the associated ranges of values assigned for calibration. Concordance of available data allows simulation over 31 years, from 1979 to 2009. Calibration is performed from 1980 to 1989 and validation, from 1990 to 2009. Each simulation is allowed an additional year for burning the model. The Pareto archived dynamically dimensioned search (PA-DDS, [37]) is used with 500 iterations to identify optimal parameter sets. A seasonal variant of Kling-Gupta-Efficiency criteria (KGE, [38]) acts as the multi-criteria objective function (OF):

$$\mathrm{OF} = \left[\mathrm{KGE}_{\mathrm{DJFMAM}}; \mathrm{KGE}_{\mathrm{JJASON}}\right] \quad (10)$$

$$\mathrm{KGE} = 1 - \sqrt{(r-1)^2 + (\alpha-1)^2 + (\beta-1)^2} \quad (11)$$

where DJFMAM refers to the period from December to May and JJASON, June to November, r, the correlation coefficient between the observed and simulated values, α, the ratio between the standard deviations, and β, the bias. All components, including KGE, target 1 as the best score.

Table 2. Hydrologic modeling setup.

Hydrologic Process	Description	Climate Input Data	Free Parameters
ET_0	Penman-Monteith	Temperature Humidity Radiation Wind speed	none
	Hamon	Temperature	f_i [0.5;2]
Precipitation correction	Separation liquid/solid precipitation	Temperature Precipitation	T_{tr} [−0.5;0.5] a_s [1;1.5]
Snow melt	T-Index degree day method	Temperature	c_0 [0;5] T_m [−2;2]
Unsaturated zone fluxes	Surface runoff generation	None	QD_{snw} [0;1]
	Interflow generation	None	d_r [1;100]
Discharge routing	Surface and interflow flow recession	None	k_s [1;100] k_h [1;150]

2.4. Correction of Simulated HRW Fields

In order to improve hydrologic performance, a calibration-based correction is applied to the simulated HRW fields such as:

$$\mathrm{H}' = \mathrm{H_s} + \mathrm{CF_{H,S}} \quad (12)$$

$$\mathrm{R}' = \mathrm{R_s} \times \mathrm{CF_{R,S}} \quad (13)$$

$$\mathrm{W}' = \mathrm{W_s} \times \mathrm{CF_{W,S}} \quad (14)$$

where $\mathrm{CF_{HRW,S}}$ are seasonal correction factors (DJFMAM vs. JJASON, additive for H and multiplicative for R and W), H′, R′ and W′, corrected fields.

Figure 2 details the calibration of the seasonal correction factors concomitantly to the free-parameters of the hydrologic model. Random initial values are used. Correction is applied to the HRW fields as prescribed by Equations (12) to (14). Corrected HRW fields are combined to observed precipitations and temperature in order to force the hydrologic model simulating streamflow. The multi-criteria objective function (Equation (10)) is computed from simulated and observed streamflow values. Calibration converges iteratively toward an optimal solution producing the final calibrated streamflow. Boundaries constraining optimized values of correction factors are here fixed at [−15%;+15%] for relative humidity and [0.75;1.25] for radiation and wind speed. Corrected relative humidity is post-processed to be bounded between 0 and 1.

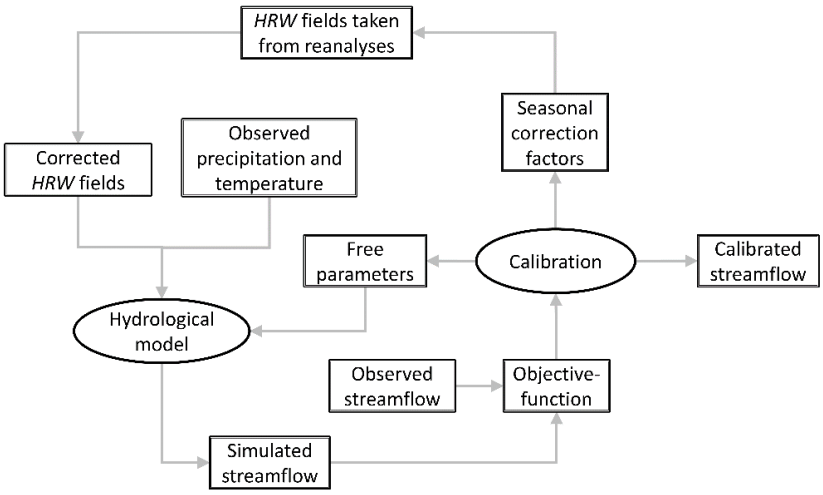

Figure 2. Calibration-based correction of HRW fields taken from reanalyses. Seasonal correction factors are calibrated concomitantly to the hydrologic model according to an objective-function, the latter minimizes deviation between observed and simulated streamflow.

3. Results

3.1. Meteorological Performance Values

Table 3 presents the meteorological performance values of CFSR, MERRA-2, ERA-Interim, and JRA-55 simulation of the humidity, radiation, and wind speed observations, while mean (M) and range (R) values synthetize the performance across all four reanalyses. Performance is expressed as KGE and its α, β and r components (Equation (11)) are evaluated from June to November between stations M1 to M5 and R1 and simulated data at the nearest grid points. All four reanalyses are more successful at simulating radiation than humidity and wind speed. Radiation performance values are mainly driven by their correlation and variance components. Humidity offers weaker correlations but good biases. Wind speed performance is less uniform in terms of bias and variance. It provides, however, relatively accurate correlations. Overall, HRW fields are quite comparable from one reanalysis to another. JRA-55 is better simulating humidity ($KGE_{JRA,H} = 0.70$) and MERRA-2, wind speed ($KGE_{MRA,W} = 0.63$). On the other hand, CFSR is less precise simulating radiation ($KGE_{CFS,R} = 0.84$).

Table 3. Meteorological performance of CFSR, MERRA-2, ERA-Interim and JRA-55 simulating humidity, radiation and wind speed observations. Performance is expressed through the Kling-Gupta efficiency metric (KGE) and its related component (α, β and r) evaluated from June to November.

	CFSR	**MERRA-2**	**ERA-Interim**	**JRA-55**	**M**	**R**
			Humidity			
KGE	0.66	0.64	0.62	0.70	0.65	0.07
α	1.19	0.82	1.25	1.04	1.07	0.43
β	1.01	1.05	0.94	0.98	0.99	0.11
r	0.72	0.70	0.73	0.71	0.71	0.02
			Radiation			
KGE	0.84	0.90	0.89	0.88	0.88	0.06
α	1.03	0.98	0.96	0.96	0.98	0.07
β	0.92	1.07	1.07	1.09	1.04	0.17
r	0.87	0.93	0.93	0.93	0.91	0.06
			Wind speed			
KGE	0.40	0.63	0.43	0.44	0.48	0.23
α	1.47	0.74	1.35	0.62	1.05	0.84
β	1.26	0.87	1.36	0.67	1.04	0.69
r	0.77	0.82	0.77	0.79	0.79	0.05

3.2. Hydrologic Performance Values

Figure 3 presents 2008 (validation) hydrographs for the raw HRW fields at sites Q1 to Q6 (Figure 1) and for CFSR, MERRA-2, ERA-Interim, and JRA-55 reanalyses. Annual KGE performance ranges from 0.53 to 0.81. Hydrographs with performance value above 0.75 generally present a more accurate representation of the spring flood. Less performing hydrographs (KGE below 0.75) tend to fail in representing either synchronism, amplitude, or volume of the spring flood. Amplitude of high flows simulated from June to November are generally underestimated, except at site Q2 that fairs better.

Figure 4 compares the performance ranges of the hydrologic model forced respectively with raw and corrected HRW fields. Performance is assessed through (validation) KGE values and related α, β and r components (Equation (11)) from December to May (DJFMAM) and from June to November (JJASON). Performance is assessed independently for all 24 combinations between six watersheds (Figure 1) and four reanalyses (Section 2.2). Distribution median values (M) are compared using the Wilcoxon rank-sum test [39] (significance level of 0.05) used by many authors to compare relative performance of hydrologic modeling approaches [8,40,41]. The corrected HRW presents a significant improvement in term of bias from June to November ($M^{\beta,\,\mathrm{raw}}_{\mathrm{JJASON}} = 1.14$, $M^{\beta,\mathrm{cor}}_{\mathrm{JJASON}} = 1.06$, $p = 0.044$). This improvement does not translate, however, into a significant increase in performance, the variance component being (not significantly) degraded. From December to May, corrected HRW fields do not affect significantly the hydrologic performance except for an outlying case ($\mathrm{KGE}_{\mathrm{DJFMAM}} = 0.22$). The latter (ERA-Interim) is affected by a degradation of the correlation component. For all other cases and for DJFMAM and JJASON period, the correlation component is not significantly affected by the correction of the HRW fields. Figure 4 also presents raw and corrected hydrologic performance values ventilated for each reanalysis ($n = 6$). Results are compared to the Hamon ET_0 formulation ($M^{\mathrm{KGE,Ham}}_{\mathrm{DJFMAM}} = 0.87$ and $M^{\mathrm{KGE,Ham}}_{\mathrm{JJASON}} = 0.66$) which also presents an outlying case ($\mathrm{KGE}_{\mathrm{DJFMAM}} = 0.45$). Even if it varies from one reanalysis to another, hydrologic performance values for the Penman-Montheith formulation can be considered equivalent to the Hamon formulation according to the Wilcoxson test.

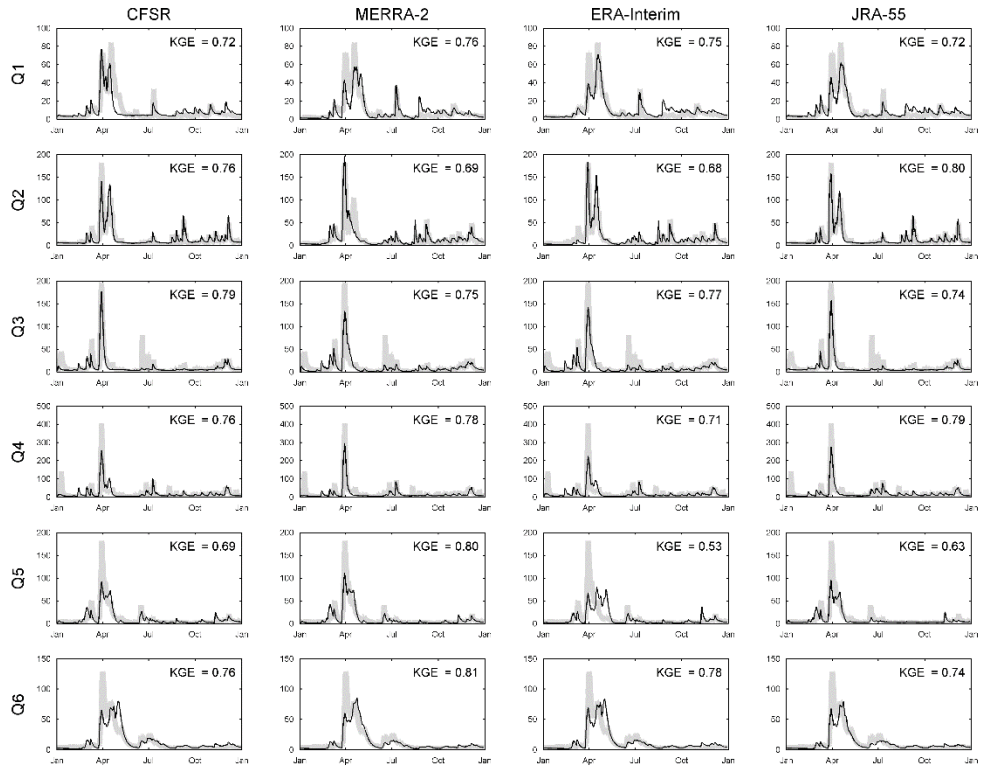

Figure 3. Observed and simulated 2008 hydrographs at sites Q1 to Q6. Hydrographs are simulated with raw HRW fields taken from CFSR, MERRA-2, ERA-Interim, and JRA-55 reanalyses.

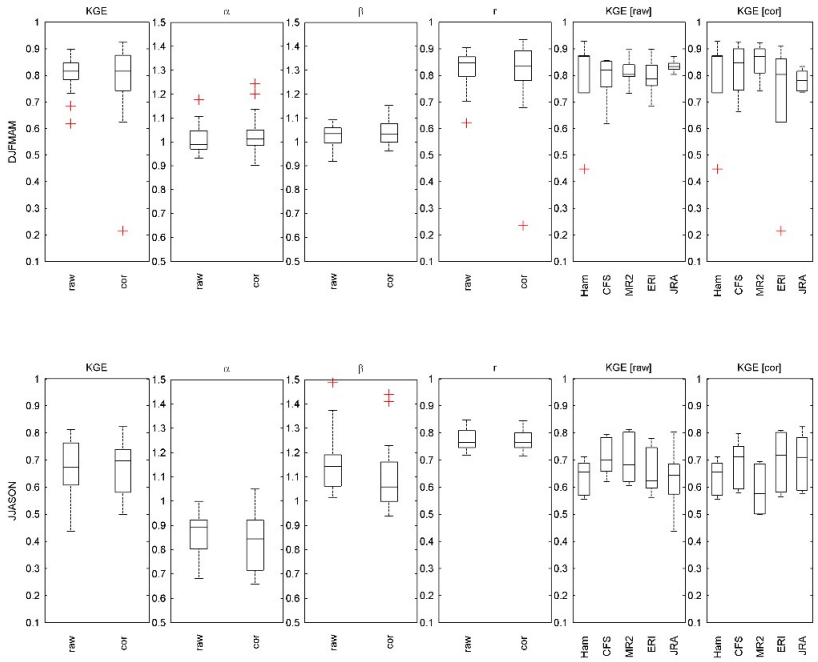

Figure 4. Hydrologic performance of the Penman-Montheith formulation forced with raw and corrected HRW fields. These latter are taken from reanalyses CFSR, MERRA-2, ERA-Interim, JRA-55 at sites Q1 to Q6 (n = 24). Performance is assessed through KGE and α, β, r components evaluated from December to May (DJFMAM) and from June to November (JJASON). KGE values are ventilated for each reanalysis and compared to the Hamon temperature-based ET_0 formulation (n = 6).

Table 4 presents the optimized values of WaSim-ETH free parameters (see also Table 2). Mean, minimal, and maximal values are presented for Hamon (n = 6 sites) and PM (n = 24 = 6 sites × 4 reanalyses), respectively forced with raw and corrected HRW fields. Mean optimized values related to Hamon tend be located around the middle of the ranges of values assigned for calibration, as defined in Table 2. Few free parameters (namely T_{tr}, T_m, d_r, and k_s) explore the margin of the defined ranges. Site-to-site variability is sporadically high ($f_{i,\mathrm{DJFMAM}}$, QD_{snw}, k_h) but much reduced in others cases (T_{tr}, a_s). Mean optimized values related to PM also tend to be centered. In most cases however, minimal and maximal optimized values are adjacent to the bounding values.

Table 4. Optimized values of WaSim-ETH free parameters.

Parameters			Hamon (n = 6)		PM Raw (n = 24)		PM Cor (n = 24)	
		Equation	Mean	[Min;Max]	Mean	[Min;Max]	Mean	[Min;Max]
$f_{i,\mathrm{DJFMAM}}$	Correction of Hamon ET_0	(3)	0.96	[0.50;1.42]	-	-	-	-
$f_{i,\mathrm{JJASON}}$			1.26	[1.14;1.40]	-	-	-	-
T_{tr}	Temperature snow/rain transition	(4)	0.42	[0.23;0.5]	0.0063	[−0.5;0.5]	0.22	[−0.44;0.5]
a_s	Correction of solid precipitation	(4)	1.28	[1.18;1.5]	1.17	[1;1.49]	1.26	[1;1.49]
c_0	Melt factor	(5)	2.61	[1.41;3.99]	2.42	[0.6;5]	2.53	[1.11;5]
T_m	Temperature limit for snow melt	(5)	−1.56	[−2;0.18]	−0.47	[−2;2]	−0.95	[−2;1.71]
QD_{snw}	Fraction of surface runoff on snow melt	(6)	0.51	[0;1]	0.67	[0;1]	0.40	[0;1]
d_r	Drainage density	(7)	81.50	[40.29;100]	33.55	[1;100]	73.12	[1;100]
k_s	Surface runoff recession constant	(8)	78.94	[51.33;100]	73.49	[28.80;100]	66.24	[30.36;100]
k_h	Inteflow recession constant	(9)	45.87	[16.65;139.82]	50.68	[11.81;150]	50.08	[10.36;150]

3.3. Simulated Evapotranspiration

Figure 5 illustrates the 2005–2009 relations between evapotranspiration (ET) and climate drivers: air temperature, relative humidity, solar radiation, and wind speed. Relations between observed variables are also presented for sites R1 (2005–2009) and R2 (2016–2018) (Figure 1). Observed ET is inferred from latent heat flux calculated from eddy correlation measurements. Daily ET observations

are generally less than 1 mm below freezing and peaks near 5 mm in summer. Above freezing, the observed ET is not strongly correlated to temperature, a notable proportion of small daily values coincide with high temperatures. The relation between observed ET and humidity decreases as humidity approaches saturation. No specific pattern emerges as humidity falls below about 75%, for which peak ET values are detected. Relation between observed ET and solar radiation reveals proportionality. ET is generally lower than 1 mm/day when radiation is below 2 kW/day, and reaches peak values above 7 kW/day. The relations between observed ET and wind speed do not present any specific pattern.

Figure 5 also presents relations between simulated ET and climate drivers. Here, ET is simulated by WaSim-ETH at site Q6 from 2005 to 2009 using Hamon and Penman-Montheith ET_0 formulations. CFSR climate drivers (raw and corrected) are used, except for temperature (in situ-observation). The Hamon formulation shows a clear exponential pattern between simulated ET and temperature. It is smaller than 1 mm/day below freezing point and reaches 6 mm/day at 25 °C. Above freezing, Hamon formulation does not reproduce low ET accurately. Moreover, it does not show any clear pattern in relation with humidity, radiation, or wind speed. Relative to observations, a notable amount of overestimated ET values are found in high humidity and low radiation situations.

PM formulation forced with raw and corrected HRW fields lead to relationships in Figure 5 that are more comparable to observations than for the Hamon formulation. Low ET values above freezing are much better represented and relations between simulated ET presents proportional patterns when in relation with humidity and radiation. Correcting HRW fields moderately modifies but does not alter the broad patterns describes previously. With temperature above freezing, simulated peak ET values are emphasised while low values are overestimated. The relation between ET and humidity is shifted left while the relation with solar radiation presents a subset of values above 7 kW/day.

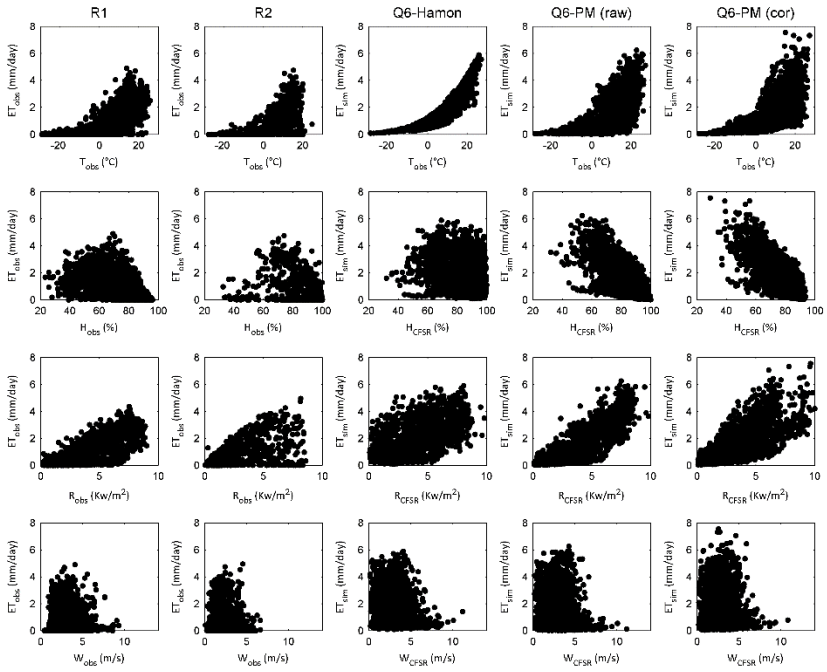

Figure 5. Relations between evapotranspiration (ET) and climate drivers: temperature (T), humidity (H), radiation (R), and wind speed (W). All variables are observed at sites R1 and R2. At site Q5, ET is simulated by WaSim-ETH with Hamon and PM formulations. T is observed and HRW are taken from CFSR reanalysis (raw and corrected).

4. Discussion

4.1. Forcing PM Formulation with Simulated HRW Fields Provides an Appropriate Hydrologic Response

The Penman-Montheith ET_0 formulation has been forced with HRW fields taken from CFSR, MERRA-2, ERA-Interim, and JRA-55 reanalyses. Hydrologic responses simulated by the WaSim-ETH model has been analyzed over six natural nivo-pluvial catchments of the St-Lawrence Valley, Canada. Results presented in Figures 3 and 4 describe site-specific and reanalysis-specific hydrologic responses that are comparable to the empirical temperature-based Hamon ET_0 formulation. During the nival period (December to May), 85% of the simulated hydrologic responses (41 out of 48, combined raw and corrected HRW) presented validation KGE above 0.70, generally depicting a sound representation of the spring flood in terms of synchronism, amplitude, and volume. Performance decreases during the pluvial season (June to November), 65% of the simulated hydrologic responses presenting KGE above 0.60. During that period, flow representation is affected by a systematic underestimation of the flow variance and a positive bias (Figure 4). These shortcomings are related to errors in the modeling setup, calibration failures identifying optimal parametric solutions, or misrepresentation in observations. The use of interpolated precipitation, which is known to smooth the amplitude of convective events common in summer and autumn, could explain part of the underestimation of the flow variance. The quality and resolution of the information describing soil textures could also affect seasonal water budgets and up to a certain extent the flow variance. Calibrating stomatal resistance could have potentially improved flow representation during the pluvial period.

The performance of reanalyses simulating HRW fields has been evaluated with available meteorological observations in Section 3.2. Reanalyses are generally better simulating solar radiation than humidity and wind speed. Simulated wind speed tends to present a strong systematic bias, potentially explained by the scaling mismatch between in-situ observations and the representation of the wind processes simulated at the grid-base resolution of a given reanalysis. Considering the absence of a pattern with observed evapotranspiration (Figure 5), the correction of wind may have been neglected in the scope of that study. Moreover, analysis of the meteorological performance did not identify the most successful reanalysis simulating HRW fields. Performance values are comparable for radiation while humidity and wind are marginally more accurately simulated by JRA-55 and MERRA-2. No evidence was found relating meteorological performance to the quality of the resulting hydrologic response. This can be explained by the parametric compensation allowing the search of an optimal solution indirectly correcting structural errors within the modeling setup. Taking this into account, validation of the resulting hydrologic response would be highly recommendable while using HRW fields simulated by reanalyses. These findings corroborate recent literature exploring the capacity of reanalyses to surrogate observations in providing an appropriate hydrological response [7–13]. They cannot highlight, as for precipitation [8,14], any strong relation between biases of raw simulated HRW fields and the quality of the resulting hydrological response.

4.2. Correcting HRW Fields Moderately Improves the Simulated Hydrologic Response

The proposed calibration-based correction has been applied to raw HRW fields in order to improve the hydrologic response. Seasonal correction factors where calibrated concomitantly to the free parameters of the hydrologic model. The correction is fairly simple to operate and does not requisite HRW observations. It relies however on the assumption that the hydrologic processes are accurate proxies of the driving climate and does not ensure the physical consistency of the corrected climate variables. In line with the work conducted by Praskievicz and Bartlein on precipitation [12], the correction provided a significant improvement of the hydrologic bias over the pluvial period (Figure 4), indicating a sensitivity of the hydrologic response to biases imprinted within HRW fields. The reduction of bias did not translate however into a significant improvement of the performance in terms of the Kling-Gupta Efficiency metric. Correction of HRW fields did not affect the simulated hydrologic responses during the nival period, except for one outlying case where correlation was highly

degraded (also observed with the Hamon ET_0 formulation). An in-depth analysis of the calibration intermediary results (not shown here for conciseness) revealed a calibration failure, identifying an optimal parametric solution.

4.3. PM Formulation Improves the Representation of Evapotranspiration

Within the scope of the study and according to the Wilcoxson test, the PM formulation does not provide a better hydrologic response relative to the Hamon formulation (Section 4.1), supporting findings from Sperna Weiland et al. [22]. Moreover, both formulations overestimate peak daily ET values (Figure 5), which suggests that the hydrologic model exploits the ET process to operate compensation in the representation of the annual water budget. However, the PM formulation provides a much better representation of low ET fluctuations associated to high temperatures. The latter, still imperfectly, constrains ET compelled by high humidity or low radiation driving conditions. On the other hand, the Hamon formulation suggests a sharp exponential relation between simulated ET and air temperature. It is unable to represent low ET fluctuations related to high air temperature, nor to constrain ET under high humidity or low radiation conditions. These results support the concerns raised in recent literature about the capacity of an empirical formulation such as Hamon in providing coherent projections of evapotranspiration in the scope of a non-stationary change of temperature [4,5]. The latter would potentially translate a projected steady increase of temperature into an exponential increase of ET. For these reasons, and considering potential changes in radiation and humidity, it seems recommendable to construct regional streamflow projections using physically-based ET_0 formulation such as Penman-Montheith. Even if the added-value is moderate in terms of hydrologic response, it would provide a more coherent representation of daily evapotranspiration fluctuations forced by increasing air temperatures.

4.4. Limitations

To further support the recommendations previously discussed, a larger set of ET_0 formulations should be analyzed. The hydrologic response is known sensible to the selection of a given ET_0 formulation [1,2]. The biases of reanalyses could also be evaluated for other regions with comparable climate but more accessible data. The PM formulation is here tested in humid climate conditions, while its capacity to simulate ET can differ in more arid conditions [42]. More sophisticated HRW correction could also have been explored taking into account more resolute annual sub-scaling, quantile sorting, or multivariate dependency between corrected climate variables. Multi-seed optimization and an increase of the optimization budget could have prevented performance degradation related to correction of HRW fields. Finally, evaluating the impact of ET_0 formulations within a complete climate change impact analysis was outside the scope of this study.

5. Conclusions

The manuscript demonstrated the capacity of the Penman-Montheith (PM) evapotranspiration formulation to provide a coherent hydrologic response when forced with HRW fields simulated by reanalyses. The resulting hydrologic performance remains however comparable to an empirical temperature-based evapotranspiration formulation and appears sensible to HRW biases. The manuscript also presented a calibration-based correction of simulated HRW fields free from observations. The latter improves significantly the hydrologic bias over the pluvial period (June to November) but not the overall performance according to the Kling-Gupta Efficiency (KGE) metric. Correction of HRW fields should be operated with caution since it can occasionally degrade the simulated hydrologic response. The PM formulation finally depicted much more consistent relations between evapotranspiration and climate drivers as compared to an empirical temperature-based evapotranspiration formulation. The manuscript proposes a pragmatic solution for computing evapotranspiration with physically-based formulations where HRW observations are insufficient. It also clarifies to which extent and under which conditions correcting HRW fields offers an improvement of the resulting hydrologic response.

To our knowledge, few studies combine HRW fields simulated by reanalyses and observed rainfall and temperature values to force hydrologic models. This approach prevents the resulting hydrologic response to be affected by strong biases inherent to precipitation simulated by reanalyses. In the scope of most climate change studies, air temperature is expected to increase steadily according to non-stationary patterns. The main interest of the proposed approach is to compute evapotranspiration by relying on a more coherent representation of physical processes, increasing the confidence in simulated projections of the hydrologic regime.

Author Contributions: Conceptualization, S.R. and F.A.; methodology, S.R. and F.A.; software, S.R.; validation, F.A.; formal analysis, S.R.; investigation, S.R.; resources, F.A.; data curation, S.R.; writing—original draft preparation, S.R.; writing—review and editing, F.A.; visualization, S.R.; supervision, F.A.; project administration, F.A.; funding acquisition, S.R. and F.A.

Funding: This research was funded by Mitacs Accelerate program for scholarship to S.R.

Acknowledgments: The authors wish to acknowledge the contributions of Ouranos and Québec Ministry of Forests, Wildlife and Parks. This work used data from one Fluxnet-Canada site in Quebec. Fluxnet-Canada was funded by NSERC, CFCAS, Biocap-Canada, and Natural Resources Canada. Authors also wish to acknowledge Quebec Ministry of Environment and Fight Against Climate Change (MELCC) for interpolated meteorological data (precipitation and temperature), hydrometric data, digital representation of the river network and integrated description of land uses. Humidity and wind data were provided by Environment and Climate Canada. The authors thank Blaise Gauvin St-Denis and Simon Lachance-Cloutier for their support.

Conflicts of Interest: The authors declare no conflict of interest.

References

1. Oudin, L.; Hervieu, F.; Michel, C.; Perrin, C.; Andréassian, V.; Anctil, F.; Loumagne, C. Which potential evapotranspiration input for a lumped rainfall-runoff model? Part 2—Towards a simple and efficient potential evapotranspiration model for rainfall-runoff modelling. *J. Hydrol.* **2005**, *303*, 290–306. [CrossRef]
2. Seiller, G.; Anctil, F. How do potential evapotranspiration formulas influence hydrological projections? *Hydrolog. Sci. J.* **2016**, *61*, 2249–2266. [CrossRef]
3. Kay, A.L.; Bell, V.A.; Blyth, E.M.; Crooks, S.M.; Davies, H.N.; Reynard, N.S. A hydrological perspective on evapotranspiration: historical trends and future projections in Britains. *J. Water Clim. Chang.* **2013**, *4*, 193–208. [CrossRef]
4. Sherwood, S.; Fu, Q. A drier future? *Science* **2014**, *343*, 737–739. [CrossRef] [PubMed]
5. Lofgren, B.M.; Gronewold, A.D.; Acciaioli, A.; Cherry, J.; Steiner, A.; Watkins, D. Methodological approaches to projecting the hydrologic impacts of climate change. *Earth Interact.* **2013**, *17*, 2–19. [CrossRef]
6. Oudin, L.; Michel, C.; Anctil, F. Which potential evapotranspiration input for a lumped rainfall-runoff model? Part 1—Can rainfall-runoff models effectively handle detailed potential evapotranspiration inputs? *J. Hydrol.* **2005**, *303*, 275–289. [CrossRef]
7. Auerbach, D.A.; Easton, Z.M.; Walter, M.T.; Flecker, A.S.; Fuka, D.R. Evaluating weather observations and the climate forecast system reanalysis as inputs for hydrologic modelling in the tropics. *Hydrol. Process.* **2016**, *30*, 3466–3477. [CrossRef]
8. Essou, G.R.C.; Sabarly, F.; Lucas-Picher, P.; Brissette, F.; Poulin, A. Can precipitation and temperature from meteorological reanalyses be used for hydrological modeling? *J. Hydrometeorol.* **2016**, *17*, 1929–1950. [CrossRef]
9. Fuka, D.R.; Walter, M.T.; MacAlister, C.; Degaetano, A.T.; Steenhuis, T.S.; Easton, Z.M. Using the climate forecast system reanalysis as weather input data for watershed Models. *Hydrol. Process.* **2014**, *28*, 5613–5623. [CrossRef]
10. Hwang, S.; Graham, W.D.; Geurink, J.S.; Adams, A. Hydrologic implications of errors in bias-corrected regional reanalysis data for west central Florida. *J. Hydrol.* **2014**, *510*, 513–529. [CrossRef]
11. Lauri, H.; Räsänen, T.A.; Kummu, M. Using reanalysis and remotely sensed temperature and precipitation data for hydrological modeling in monsoon climate: Mekong river case study. *J. Hydrometeorol.* **2014**, *15*, 1532–1545. [CrossRef]
12. Praskievicz, S.; Bartlein, P. Hydrologic Modeling Using Elevationally Adjusted NARR and NARCCAP regional climate-model simulations: Tucannon River, Washington. *J. Hydrol.* **2014**, *517*, 803–814. [CrossRef]

13. Seyyedi, H.; Anagnostou, E.N.; Beighley, E.; McCollum, J. Hydrologic evaluation of satellite and reanalysis precipitation datasets over a mid-latitude basin. *Atmos. Res.* **2015**, *164–165*, 37–48. [CrossRef]
14. Xu, H.; Xu, C.Y.; Chen, S.; Chen, H. Similarity and difference of global reanalysis datasets (WFD and APHRODITE) in driving lumped and distributed hydrological models in a humid region of China. *J. Hydrol.* **2016**, *542*, 343–356. [CrossRef]
15. Boulard, D.; Castel, T.; Camberlin, P.; Sergent, A.S.; Bréda, N.; Badeau, V.; Rossi, A.; Pohl, B. Capability of a regional climate model to simulate climate variables requested for water balance computation: A case study over northeastern France. *Clim. Dyn.* **2016**, *46*, 2689–2716. [CrossRef]
16. Canon, D.J.; Brayshaw, D.J.; Methven, J.; Coker, P.J.; Lenaghan, D. Using reanalysis data to quantify extreme wind power generation statistics: A 33 year case study in Great Britain. *Ren. Energy* **2015**, *75*, 767–778. [CrossRef]
17. Stopa, J.E.; Cheung, K.F. Intercomparison of wind and wave data from the ECMWF reanalysis interim and the NCEP climate forecast system reanalysis. *Ocean Model.* **2014**, *75*, 65–83. [CrossRef]
18. Mao, Y.; Wang, K. Comparison of evapotranspiration estimates based on the surface water balance, modified penman-monteith model, and reanalysis data sets for continental China. *J. Geophys. Res. Atmos.* **2017**, *122*, 3228–3244. [CrossRef]
19. Martins, D.S.; Paredes, P.; Raziei, T.; Pires, C.; Cadima, J.; Pereira, L.S. Assessing reference evapotranspiration estimation from reanalysis weather products. An application to the Iberian Peninsula. *Int. J. Climatol.* **2017**, *37*, 2378–2397. [CrossRef]
20. Huang, S.Y.; Deng, Y.; Wang, J. Revisiting the global surface energy budgets with maximum-entropy-production model of surface heat fluxes. *Clim. Dyn.* **2017**, *49*, 1531–1545. [CrossRef]
21. Yao, Y.; Zhao, S.; Zhang, Y.; Jia, K.; Liu, M. Spatial and decadal variations in potential evapotranspiration of china based on reanalysis datasets during 1982–2010. *Atmosphere* **2014**, *5*, 737–754. [CrossRef]
22. Sperna Weiland, F.C.; Tisseuil, C.; Dürr, H.H.; Vrac, M.; Van Beek, L.P.H. Selecting the optimal method to calculate daily global reference potential evaporation from CFSR reanalysis data for application in a hydrological model study. *Hydrol. Earth Syst. Sci.* **2012**, *16*, 983–1000. [CrossRef]
23. Jones, P.D.; Harpham, C.; Troccoli, A.; Gschwind, B.; Ranchin, T.; Wald, L.; Goodess, C.M.; Dorling, S. Using ERA-interim reanalysis for creating datasets of energy-relevant climate variables. *Earth Syst. Sci. Data* **2017**, *9*, 471–495. [CrossRef]
24. Sen Gupta, A.; Tarboton, D.G. A Tool for Downscaling weather data from large-grid reanalysis products to finer spatial scales for distributed hydrological applications. *Environ. Modell. Softw.* **2016**, *84*, 50–69. [CrossRef]
25. Essou, G.R.C.; Brissette, F.; Lucas-Picher, P. Impacts of combining reanalyses and weather station data on the accuracy of discharge modelling. *J. Hydrol.* **2017**, *545*, 120–131. [CrossRef]
26. Mailhot, A.; Talbot, G.; Ricard, S.; Turcotte, R.; Guinard, K. Assessing the potential impacts of dam operation on daily flow at ungauged river reaches. *J. Hydrol. Regional Stud.* **2018**, *18*, 156–167. [CrossRef]
27. Saha, S.; Moorthi, S.; Wu, X.; Wang, J.; Nadiga, S.; Tripp, P.; Behringer, D.; Hou, Y.T.; Chuang, H.Y.; Iredell, M.; et al. The NCEP climate forecast system version 2. *J. Clim.* **2014**, *27*, 2185–2208. [CrossRef]
28. Gelaro, R.; McCarty, W.; Suárez, M.J.; Tolding, R.; Molod, A.; Takacs, L.; Randles, C.A.; Darmenov, A.; Bosilovich, M.G.; Reichle, R.; et al. The modern-era retrospective analysis for research and applications, version 2 (MERRA-2). *J. Climate* **2017**, *30*, 5419–5454. [CrossRef]
29. Dee, D.P.; Uppala, S.M.; Simmons, A.J.; Berrisford, P.; Poli, P.; Kobayashi, S.; Andrae, U.; Balmaseda, M.A.; Balsamo, G.; Bauer, P.; et al. The ERA-interim reanalysis: Configuration and performance of the data assimilation system. *QJR Meteorol. Soc.* **2011**, *137*, 553–597. [CrossRef]
30. Chen, G.; Iwasaki, T.; Qin, H.; Sha, W. Evaluation of the warm-season diurnal variability over east asia in recent reanalyses JRA-55, ERA-interim, NCEP CFSR, and NASA MERRA. *J. Clim.* **2014**, *27*, 5517–5537. [CrossRef]
31. Kobayashi, S.; Ota, Y.; Harada, Y.; Ebita, A.; Moriya, M.; Onoda, H.; Onogi, K.; Kamahori, H.; Kobayashi, C.; Endo, H.; et al. The JRA-55 reanalysis: General specifications and basic characteristics. *J. Meteorol. Soc. Jpn.* **2015**, *93*, 5–48. [CrossRef]
32. Cornelissen, T.; Diekkrüger, B.; Giertz, S. A comparison of hydrological models for assessing the impact of land use and climate change on discharge in a tropical catchment. *J. Hydrol.* **2013**, *498*, 221–236. [CrossRef]

33. Ott, I.; Duethmann, D.; Liebert, J.; Berg, P.; Feldmann, H.; Ihringer, J.; Kunstmann, H.; Merz, B.; Schaedler, G.; Wagner, S. High-resolution climate change impact analysis on medium-sized river catchments in germany: an ensemble assessment. *J. Hydrometeorol.* **2013**, *14*, 1175–1193. [CrossRef]
34. Smiatek, G.; Kunstmann, H.; Werhahn, J. Implementation and performance analysis of a high resolution coupled numerical weather and river runoff prediction model system for an alpine catchment. *Environ. Modell. Softw.* **2012**, *38*, 231–243. [CrossRef]
35. Allen, R.G.; Pereira, L.S.; Raes, D.; Smith, S. *Crop Evapotranspiration—Guidelines for Computing Crop Water Requirements*; Irrigation and Drainage Paper 56; FAO: Rome, Italy, 1998; pp. 1–15.
36. Shangguan, W.; Dai, Y.; Duan, Q.; Liu, B.; Yuan, H. A global soil data set for earth system modeling. *J. Adv. Model. Earth Syst.* **2014**, *6*, 249–263. [CrossRef]
37. Asadzadeh, M.; Tolson, B.A. Hybrid pareto archived dynamically dimensioned search for multi-objective combinatorial optimization: application to water distribution network design. *J. Hydroinform.* **2012**, *14*, 192–205. [CrossRef]
38. Gupta, H.V.; Kling, H.; Yilmaz, K.K.; Martinez, G.F. Decomposition of the mean squared error and nse performance criteria: Implications for improving hydrological modelling. *J. Hydrol.* **2009**, *377*, 80–91. [CrossRef]
39. Wilcoxon, F. Individual comparisons by ranking methods. *Biometrics* **1945**, *1*, 80–83. [CrossRef]
40. Muerth, M.J.; Gauvin St-Denis, B.; Ricard, S.; Velázquez, J.A.; Schmid, J.; Minville, M.; Caya, D.; Chaumont, D.; Ludwig, R.; Turcotte, R. On the need for bias correction in regional climate scenarios to assess climate change impacts on river runoff. *Hydrol. Earth Syst. Sci.* **2013**, *17*, 1189–1204. [CrossRef]
41. Velázquez, J.A.; Schmid, J.; Ricard, S.; Muerth, M.J.; Gauvin St-Denis, B.; Minville, M.; Caya, D.; Chaumont, D.; Ludwig, R.; Turcotte, R. An ensemble approach to assess hydrological models' contribution to uncertainties in the analysis of climate change impact on water resources. *Hydrol. Earth Syst. Sci.* **2013**, *17*, 565–578. [CrossRef]
42. Hajji, I.; Nadeau, D.F.; Music, B.; Anctil, F.; Wang, J. Application of the maximum entropy production model of evapotranspiration over partially vegetated water-limited land surfaces. *J. Hydrometeorol.* **2019**, *19*, 989–1005. [CrossRef]

Annexe 2 : Article publié dans la revue *Water* en septembre 2019

water

MDPI

Article

Exploring an Alternative Configuration of the Hydroclimatic Modeling Chain, Based on the Notion of Asynchronous Objective Functions

Simon Ricard [1,*], Jean-Daniel Sylvain [2] and François Anctil [1]

[1] Department of Civil and Water Engineering, Laval University, Québec, QC G1V 0A6, Canada; Francois.Anctil@gci.ulaval.ca

[2] Direction de la recherche forestière, Ministère des Forêts, de la Faune et des Parcs, Québec, QC G1P 3W8, Canada; jean-daniel.sylvain@mffp.gouv.qc.ca

* Correspondence: simon.ricard.1@ulaval.ca

Received: 8 August 2019; Accepted: 25 September 2019; Published: 27 September 2019

Abstract: This study explores an alternative configuration of the hydroclimatic modeling chain around the notion of asynchronous objective-function (AOF). AOFs are calibration criteria purposely ignoring the correlation between observed and simulated variables. Within the suggested alternative configuration, the hydrologic model is being forced and calibrated with bias corrected climate variables over the reference period instead of historical meteorological observations. Consequently, the alternative configuration circumvent the redundant usage of climate observation operated within conventional configurations for statistical post-processing of simulated climate variables and calibration of the hydrologic model. AOFs optimize statistical properties of hydroclimatic projections, preserving the sequence of events imbedded within the forcing climate model. Both conventional and alternative configurations of the hydroclimatic modeling chain are implemented over a mid-size nivo-pluvial catchment located in the Saint-Lawrence Valley, Canada. The WaSiM-ETH hydrological model is forced with a bias-corrected member of the Canadian Regional Climate Model Large Ensemble (CRCM5-LE). Five AOFs are designed and compared to the common Kling-Gupta efficiency (KGE) metric. Forced with observations, AOFs tend to provide a hydrologic response comparable to KGE during the nival season and moderately degraded during the pluvial season. Using AOFs, the alternative configuration of the hydroclimatic modeling chain provides more coherent hydrologic projections relative to a conventional configuration.

Keywords: hydroclimatology; modeling chain; objective functions; catchment scale

1. Introduction

Many studies assess the impact of climate change on regional water flow regimes by implementing a hydroclimatic modeling chain [1–6] that translates climate variables projected by Global Climate Models (GCM) or Regional Climate Models (RCM) into the future hydrologic regime of a given watershed. Conventional configurations of the hydroclimatic chain (Figure 1) first apply statistical post-processing to simulated climate variables in order to minimize mismatches with observations. Quantile mapping [7,8] is a common post-processing method which defines transfer functions that relate empirical distributions of climate observations and simulations over an overlapping reference period. Corrected climate variables over reference and future periods are then produced applying the transfer function to raw simulations. In parallel, a hydrologic model is forced with climate observations, simulating hydrologic processes at the catchment scale. Through an iterative process, an optimization algorithm calibrates the free parameters of the hydrologic model according to a given objective-function:

A criterion minimising the error between simulated and observed streamflow. Hydrologic projections over reference and future periods are finally produced forcing the calibrated hydrologic model with the corrected climate variables.

Albeit frequently used to assess the impact of climate change on water resources, conventional configurations of hydroclimatic chains raise concerns regarding their ability in producing consistent hydrologic projections. These latter operate quantile mapping and calibration independently without ensuring consistency between the redundant usages of climate observations (dashed lines, Figure 1). Climate data heterogeneity and scarcity are among the most important limitations of hydroclimatic modeling [9–11], motivating the use of modeling chains that rely exclusively on air temperature and precipitation. Surrogating the deficient observation coverage by biased reanalyses or remote sensing products often corrode the resulting simulated hydrological response [12,13]. In this context, avoiding a non-added-value redundant use of climate observation may potentially lead to a reduction of the overall uncertainty affecting the hydroclimatic modeling chain [14,15].

In opposition to meteorological applications, climate modeling is not constantly updated in order to better reproduce the observed conditions of the climate system, these latter being exclusively imposed at the onset of the projection run. It has for consequence that simulated climate series rapidly depart from the sequence of observed climate events over the historical period (meteorology) but the statistical properties of the climate system is preserved over a few decades [16]. Applied to simulated climate time series, quantile mapping conducts an asynchronous transformation which preserves the sequence of events embedded within the climate model [17]. In contrast, hydrologic models are typically trained in reproducing the sequence of events observed over the historical period. Since most climate change impact studies on water resources assess the projected change in statistical properties between a reference and a future simulated flow regime [18], the use of the correlation component in the objective functions appears questionable. Does it bring added-value to the resulting hydrologic projections? Or on the other hand, does it taints the parametric identity of the calibrated model in a way that would corrode the credibility of the resulting projections [19]? The redundant use of climate observations may also be circumvented using bottom-up vulnerability-based (scenario-free) approaches assessing the impact of climate changes on water resources [20–22].

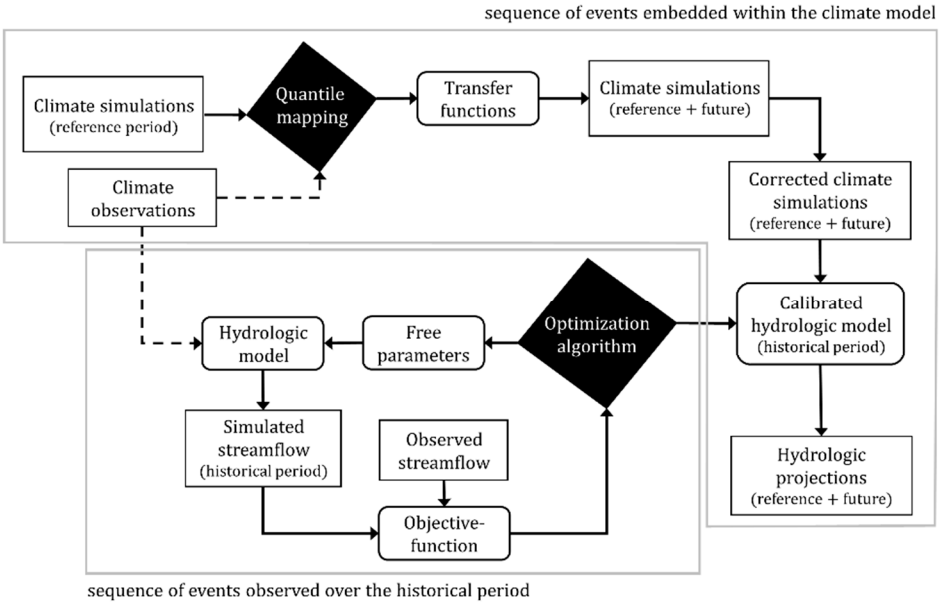

Figure 1. A conventional configuration of a hydroclimatic modeling chain.

In this study, we propose an alternative configuration of the hydroclimatic modeling chain that forces and calibrates the hydrologic model directly with post-processed climate simulations, instead of observations (Figure 2). Since the sequence of events embedded within the climate model differs

from historical observations, a calibration criteria must purposely ignore correlation between observed and simulated streamflow. Such a criteria is hereafter referred to as "asynchronous objective-function" (AOF, defined in Section 2.1). We first evaluate in Section 3.1 the hydrological performance of five exploratory AOFs forcing the WaSiM-ETH hydrologic model with climate observations over three mid-size catchments located in the St. Lawrence Valley, Canada (Section 2.3). We subsequently examine the capacity of the alternative configuration in constructing consistent hydrologic projections over the reference period simulated by the climate model (Section 3.2). We expect correlation-based calibration to dominate AOFs over the observed historical period, whereas AOFs provide more accurate hydrologic projections. The scope of the study remains a proof a concept aiming to define the notion of asynchronous objective functions (AOFs) and demonstrating its applicability in the scope of climate change impact studies.

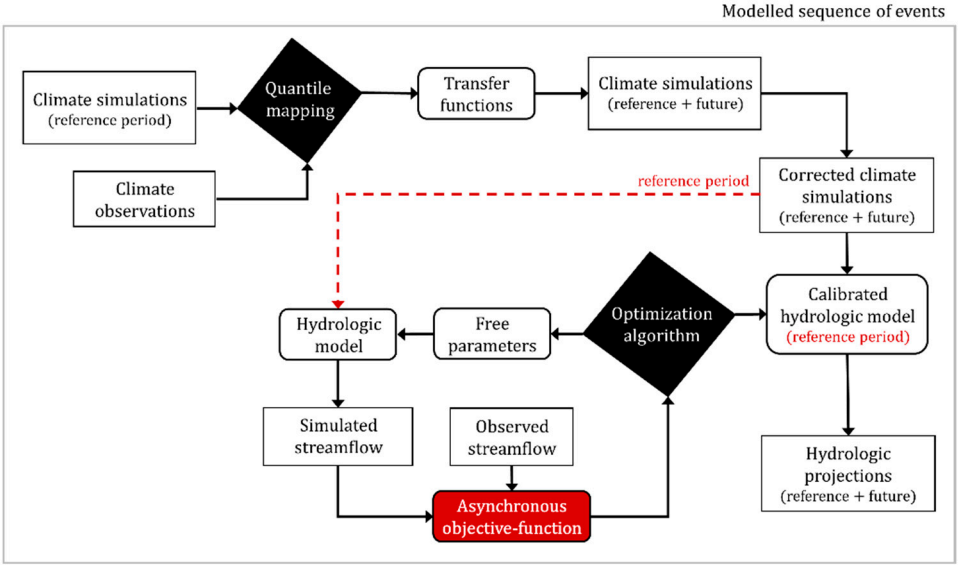

Figure 2. Alternative configuration of the hydroclimatic modeling chain.

2. Methodology

The proposed step-by-step methodological framework (detailed in Appendix A) aims firstly at the testing of five exploratory AOFs in a standard modeling framework: The hydrologic model is forced with climate observations and performance is evaluated between synchronized observed and simulated streamflow values. AOFs are compared to the KGE metric over three catchments using a common split-sample test. Any AOFs presenting inappropriate performance will then be excluded from further analysis. A site-to-site variability of the simulated hydrological response is performed next to confirm the good behavior of the modeling chain before it full application to a single site. Hydrological projections are subsequently constructed from climate model simulations. Since projections are not synchronized to observations, performance is evaluated using statistical criteria excluding correlation. The evaluation of the split sample-sample test (calibration/validation periods) remains consistent with previous analyses.

2.1. Asynchronous Objective Functions

Commonly referred to as 'calibration metrics' or 'optimization metrics', objective functions are goodness-of-fit measures orienting a calibration process toward an optimal parametric solution. The numerous calibration metrics described in the literature [23] are used individually or in a group of two or three [24–26]. It is also possible to transform the streamflow time series prior to using a metric in order to attribute more weights to high, intermediate, or low flows [27]. The selection of a given objective-function is known to affect the response simulated by a hydrologic model forced with either

climate observations [28,29] or climate model simulations [27,30,31]. Most common calibration metrics, among which the root mean square deviation (RMSD, [32]), Nash–Sutcliffe efficiency (NSE, [33]) and Kling–Gupta efficiency (KGE, [34]), contain a correlation component, which means they are designed to provide an optimized simulated time series synchronized with observations.

Asynchronous objective functions (AOFs) are here defined as calibration metrics that purposely neglects to account for the correlation between the observed and simulated variables. AOFs rather minimize deviations of other statistical properties between the observed and simulated variables. Five exploratory AOFs are described in Table 1 and tested in Section 3. *AOF1* refers to the root mean square deviation applied to the interannual hydrograph (Equation (1)):

$$AOF1 = \sqrt{\frac{\sum_{i=1}^{365}\left(\overline{Q_{obs,i}} - \overline{Q_{sim,i}}\right)^2}{365}} \quad (1)$$

where $\overline{Q_{obs,i}}$ and $\overline{Q_{sim,i}}$ are observed and simulated mean annual streamflow, and i, the day of the year.

AOF1 relies on the assumption that the hydrologic regime associated to the climate model should be imprinted with statistical properties comparable to observations, notwithstanding the distinct sequence of daily events. *AOF2* seeks minimizing the absolute deviation (*AD*) in the n-th moments of the observed and simulated streamflow distributions (Equation (2)):

$$AOF2 = AD_{n,t} = \left|\mu_{n,t}^{sim} - \mu_{n,t}^{obs}\right| \quad (2)$$

AOF3 refers to the absolute deviation (*AD*) between mean values (μ_1) for the m-quantiles of the simulated and observed distributions (Equation (3)):

$$AOF3 = AD_m = \left|\mu_{1,m}^{sim} - \mu_{1,m}^{obs}\right| \quad (3)$$

AOF4 and *AOF5* (Equations (4) and (5)) result from the combinations of *AOF1* with *AOF2* and *AOF3*, respectively:

$$AOF4 = [AOF1; AOF2] \quad (4)$$

$$AOF5 = [AOF1; AOF3] \quad (5)$$

AOF1 is the most straightforward AOF since it is constructed through a single optimisation criteria and does not require a Pareto-based optimisation algorithm in opposition to others AOFs. *AOF2* is configured to optimise the first three moments: Mean, variance and skewness (n = 1 to 3, Table 1). A biannual sub-scaling (t = 2) preprocessing is applied, so the moments are optimised distinctly for the nival (December to May, DJFMAM) and pluvial seasons (June to November, JJASON, see Section 2.3 for a description of the hydrologic regime). The resulting number of optimisation criteria for *AOF2* thus reaches 6. *AOF3* is configured to optimise the mean values of five quantiles from the streamflow distributions (m = 1–5 without any temporal sub-scaling, thus five optimisation criteria). Since *AOF1* is equivalent to a first order criteria, we excluded the first moment (n = 1) from *AOF4* and the 50th percentile value (m = 3) from *AOF5* to avoid the potential redundancy.

Table 1. Description and configuration of asynchronous objective functions (AOFs).

	Description	Equation	Configuration	Number of Criteria
AOF1	Root mean square deviation (RMSD) between observed ($\overline{Q_{obs,i}}$) and simulated mean annual streamflow ($\overline{Q_{sim,i}}$), where i is the day of the year.	(1)	-	1
AOF2	Absolute deviation (AD) of n-th moments (μ_n) with temporal sub-scaling (t)	(2)	n = 1–3 t = 2	6
AOF3	Absolute deviation (AD) of the m-th quantiles mean values (μ_1)	(3)	m = 1 to 5	5
AOF4	Combination of *AOF1* and *AOF2*	(4)	n = 2, 3 t = 2	5
AOF5	Combination of *AOF1* and *AOF3*	(5)	m = 1, 2, 4, 5	5

2.2. Alternative Configuration of the Hydroclimatic Modeling Chain

Figure 2 (see Introduction) depicts the proposed alternative configuration of the hydroclimatic modeling chain, which aims to circumvent the typical redundant usage of the climate observations that affect conventional configurations (Figure 1). Quantile mapping of simulated climate variables is operated identically to the conventional configuration. The hydrologic model is forced however with corrected climate variables over the reference period and calibrated according to a given asynchronous objective-function (AOF, Section 2.1). The latter minimises statistical deviations between simulated hydrologic projections over the reference period and their corresponding observations. Hydrologic projections are produced by forcing the hydrologic model calibrated over the modeled reference period with corrected climate variables. In opposition to the conventional configuration of the hydroclimatic modeling chain, the alternative configuration do only requisite a single usage of the climate observations, it is fully operated within the sequence of events embedded within the climate model. Forcing and calibrating hydrologic models with simulated climate variables remains a marginal practice, but is yet documented in literature [35].

2.3. Domain, Data, and Modeling Setup

Asynchronous objective functions are tested over three intermediate size catchments (515–633 km^2) located in the St. Lawrence River Valley, Southern Quebec, Canada (Figure 3). Catchments are characterized by a nivo-pluvial hydrologic regime and a moderate slopes (5.9–6.4%). Forest is the dominant land cover type (59–77%) along with regenerating forest, wetlands and agriculture. The total annual precipitation is roughly 1000 mm while mean air temperature varies from −12 °C in January to 18 °C in July. Daily precipitation and temperature observations are interpolated by kriging to 0.1 degree, from in situ observations. Daily streamflow observations are extracted from hydrometric stations 022507 (Du Loup, 47.61° N, −69.64° E), 030101 (Nicolet Sud-Ouest, 45.80° N, −72.00° E) and 052233 (De l'Achigan, 45.90° N, −73.50° E).

The physically-based distributed hydrologic model WaSiM-ETH [36,37] was implemented over Du Loup, Nicolet Sud-Ouest and De l'Achiguan catchments (Figure 3, further details on the modeling setup are provided by Ricard and Anctil [13]). The river network is generated from a burned 50-m resolution digital elevation model (Figure 4a, Du Loup catchment is given as an example), resampled to 500 m and manually corrected. Land use is extracted from various sources provided by local agencies (Figure 4b). Percentages of clay, silt, and sand (Figure 4c) were retrieved from soil textures defined by Shangguan et al. [38].

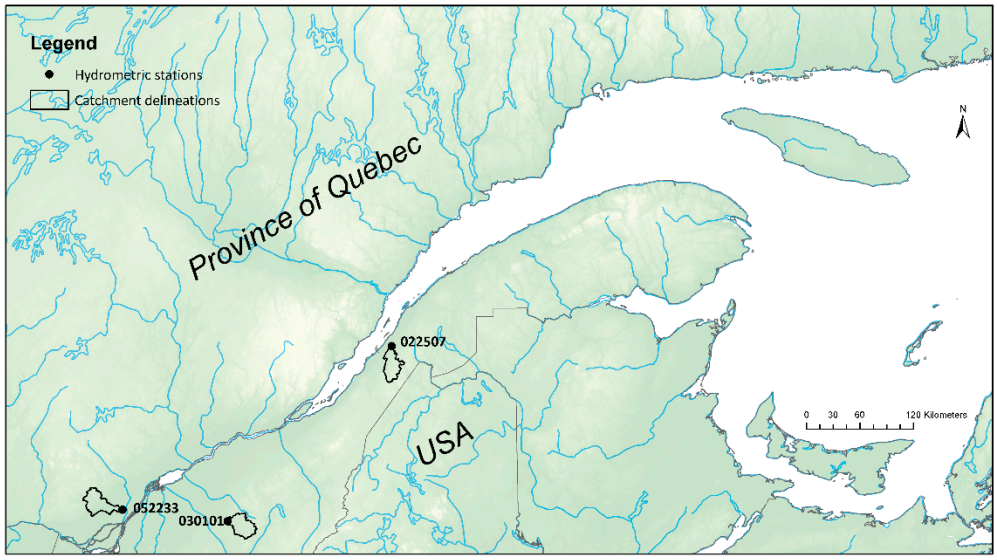

Figure 3. Du Loup (022507), Nicolet Sud-Ouest (030101) and De l'Achigan (052233) catchments.

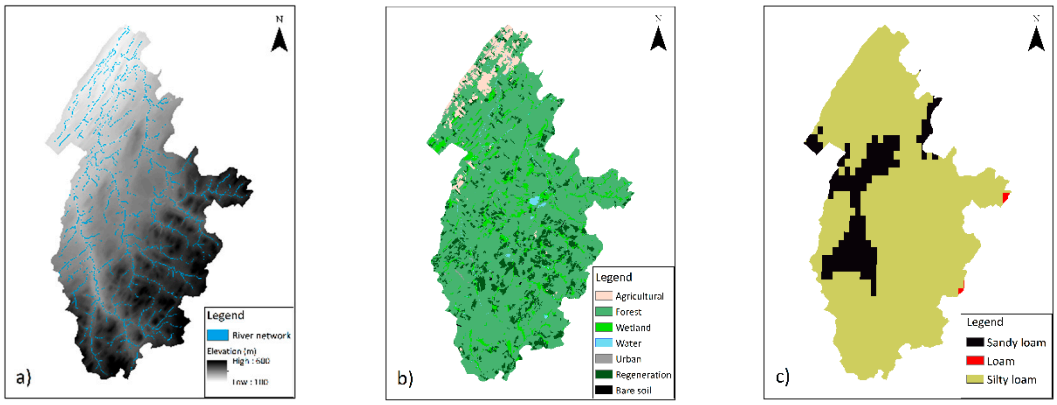

(**a**) (**b**) (**c**)

Figure 4. Du Loup River catchment (515 km^2). (**a**) Topography and river network, (**b**) land uses, and (**c**) soil textures.

Reference evapotranspiration (E_0) is evaluated using the Hamon temperature-based empirical formulation [39]:

$$E_0 = 0.1651 \cdot f_i \cdot \frac{h_d}{12} \cdot \frac{216.6 \cdot e_s}{T + 273.3} \quad (6)$$

where f_i is an empirical correction factor (-), h_d is the day length (h), and e_s is the saturation vapor pressure at temperature T (hPa).

Snowmelt is simulated using a temperature-index degree-day method [36]:

$$M = c_0(T - T_m) \cdot \frac{\Delta t}{24} \quad (7)$$

where M is the melting rate (mm·d^{-1}), c_0 is a temperature-dependent melt factor (mm·°C^{-1}·d^{-1}), T_m is the temperature limit for snow melt (°C), and Δt is the time step (h).

Vertical fluxes within the unsaturated zone are based on Richards equation [40] applied to a 10-m deep column composed of 30 numeric layers. Surface runoff is a function of precipitation intensity

and hydraulic conductivity, while transient soil hydraulic properties follow the Van Genuchten equations [41]. The fraction of snow melt taken as surface runoff (QD_{snw}) is defined empirically [36]:

$$Q_s = Q_{snw} \cdot QD_{snw} \tag{8}$$

where Q_s is the surface runoff (mm) and Q_{snw} is the snow melt (mm).

Interflow (Q_{int}) is generated at soil layer boundaries considering slope and hydraulic conductivity [38]:

$$Q_{int} = k_s(\theta_m) \cdot \Delta z \cdot d_r \tan(\beta) \tag{9}$$

where k_s, the saturated hydraulic conductivity (ms^{-1}), θ_m is the water content in layer m (-), Δz is the layer thickness (m), d_r is a scaling parameter to consider river density (m^{-1}), and β is the local slope angle (°).

Both surface runoff and interflow are delayed using recession constants [36]:

$$Q_{s,i} = Q_{s,i-1} \cdot e^{-\Delta t/k_s} + Q_s \cdot \left(1 - e^{-\Delta t/k_s}\right) \tag{10}$$

$$Q_{h,i} = Q_{h,i-1} \cdot e^{-\Delta t/k_h} + Q_h \cdot \left(1 - e^{-\Delta t/k_h}\right) \tag{11}$$

where $Q_{s,i}$ and $Q_{h,i}$ are delayed surface runoff and interflow at time step i (mm), Q_s and Q_h are the surface runoff and interflow at time step i (mm), Δt is the time step (h), and k_s and k_h are recession constants (h).

Calibration of the model is operated using the Pareto Archived Dynamically Dimensioned Search optimization algorithm (PA-DDS, [42]) applied to the eight free parameters described in Table 2. Calibration is operated from 1980 to 1989 with a 1500-iteration budget. Validation is computed using the 1990–2009 period. For all simulations, we allowed an additional year for burning the hydrologic model. AOFs are evaluated in Section 3, relative to a seasonal variation of the Kling–Gupta efficiency (KGE_s, [26]):

$$KGE_s = \left[KGE_{DJFMAM}; KGE_{JJASON}\right] \tag{12}$$

$$KGE = 1 - \sqrt{(r-1)^2 + (\propto -1)^2 + (\beta - 1)^2} \tag{13}$$

where DJFMAM refers to the period from December to May and JJASON, June–November, r is the correlation coefficient between the observed and simulated values, α is the ratio between the standard deviations, and β is the bias. All components, including KGE, target 1 as the best score.

Simulated climate variables are extracted from the Canadian Regional Climate Model Large Ensemble (CRCM5-LE, [43]). The latter consists in the dynamical downscaling of the 50-member CanESM2-Large ensemble [44] using the CRCM5 [45] at a 12-km resolution over Northeastern North America. Climate simulations run from 1950 to 2100 following RCP8.5. For the purpose of the present study, daily mean air temperature and total precipitation are taken from the first member. Univariate quantile mapping is applied to simulated precipitation and temperature with a 50-bin transfer function, a monthly sub-scaling, and a three-month moving window. Precipitation below 1 mm is excluded from the calculation of the transfer function in order to prevent the 'drizzle effect' [46]. An additive correction is applied to air temperature while a multiplicative correction is applied to precipitation.

Table 2. Calibration parameters.

Module	Calibration Parameter	Description	Unit	Boundaries
Reference evapotranspiration	f_i	Seasonal correction factors (DJFMAM, JJASON)	(-)	[0.5;2]
Snow accumulation and melt	c_0	Temperature-dependent melt factor	($mm \cdot °C^{-1} \cdot d^{-1}$)	[0;5]
	T_m	Temperature limit for snow melt	(°C)	[−2;2]
Unsaturated zone fluxes	QD_{snw}	Fraction of surface runoff on snow melt	(-)	[0;1]
	d_r	Scaling parameter for river density	(m^{-1})	[1;100]
	k_s	Surface runoff recession constant	(h)	[1;100]
	k_h	Interflow recession constant	(h)	[1;150]

3. Results

In Section 3.1, the hydrologic model is forced with climate observations over three catchments (Figure 3). In this common setup, observed and simulated streamflow values are synchronized. It is thus expected that a calibration based on the KGE_s should dominate the AOFs, the former includes a correlation component. In Section 3.2, hydrologic projections are constructed over the climatic reference period for a single catchment. Configurations of the modeling chain are constructed using KGE_s and most performing AOFs. In this case, it is hypothesized that the AOFs would do better because of the lack of synchronicity between the observed streamflow and the simulated climate time series.

3.1. Hydrological Performance over the Historical Period

Figure 5 presents the Du Loup River interannual and annual hydrographs (1990, 1995, 2000, and 2005) in validation, simulated by the WaSiM-ETH model forced and calibrated with historical meteorological observations. Calibration is steered either with KGE_s (Equation (12)) or with asynchronous objective functions *AOF1–AOF5* (Section 2.1). The interannual performance is expressed in terms of *RMSD* (Equation (1), *RMSD* = 0 in case of perfect agreement) and the annual performance, in terms of KGE (Equation (13), which target = 1). Results show that KGE_s calibration provides an accurate representation of the interannual hydrograph ($RMSD_{hst,KGEs}$ = 1.84 m^3/s), with annual performance (KGE) ranging from 0.64 to 0.77. The synchronism of the nival peak flows is accurately represented but amplitudes are generally underestimated (1995, 2000, and 2005). *AOF1* leads to a hydrologic performance comparable to KGE_s. Synchronicity of the interannual hydrograph is marginally improved ($RMSD_{hst,AOF1}$ = 1.30 m^3/s). *AOF1* annual performance improves in most cases (1995, 2000 and 2005), ranging from 0.75 to 0.86, since *AOF1* tends to improve the synchronicity of simulated nival peak flows but to degrade flow variance during the pluvial season, relative to the KGE_s. *AOF2* offers a much poorer representation of the interannual hydrograph ($RMSD_{hst,AOF2}$ = 10.4 m^3/s). Annual performance falls to 0.37 from 0.66 mostly because the simulated nival peak flows are systematically overestimated or out of phase, while the pluvial season variance is underestimated. *AOF3* also offers a poor representation of the interannual hydrograph ($RMSD_{hst,AOF3}$ = 4.38 m^3/s). Annual performance ranges from 0.35 to 0.70 mostly because the simulated nival peak flows are underestimated, while the pluvial season variance is improved relative to *AOF1*. *AOF4* leads to a moderately degraded interannual hydrograph ($RMSD_{hst,AOF4}$ = 3.22 m^3/s). The amplitude of the mean annual nival peak flow is slightly overestimated while its recession synchronicity, out of phase.

Some annual hydrographs are improvements over the KGE*s* (1995, 2000, and 2005) but not systematically (1990). Flow variance is more accurate than other objectives-functions during the pluvial season. *AOF5* allows marginal improvements of annual hydrograph over KGE*s* ($RMSD_{hst,AOF5}$ = 1.62 m^3/s). Its annual performance is also very similar to *AOF1*, ranging from 0.75 to 0.89. It generally provides a robust representation of nival peak flows in terms of amplitude, timing, and volume, but it underestimates the pluvial flow variance.

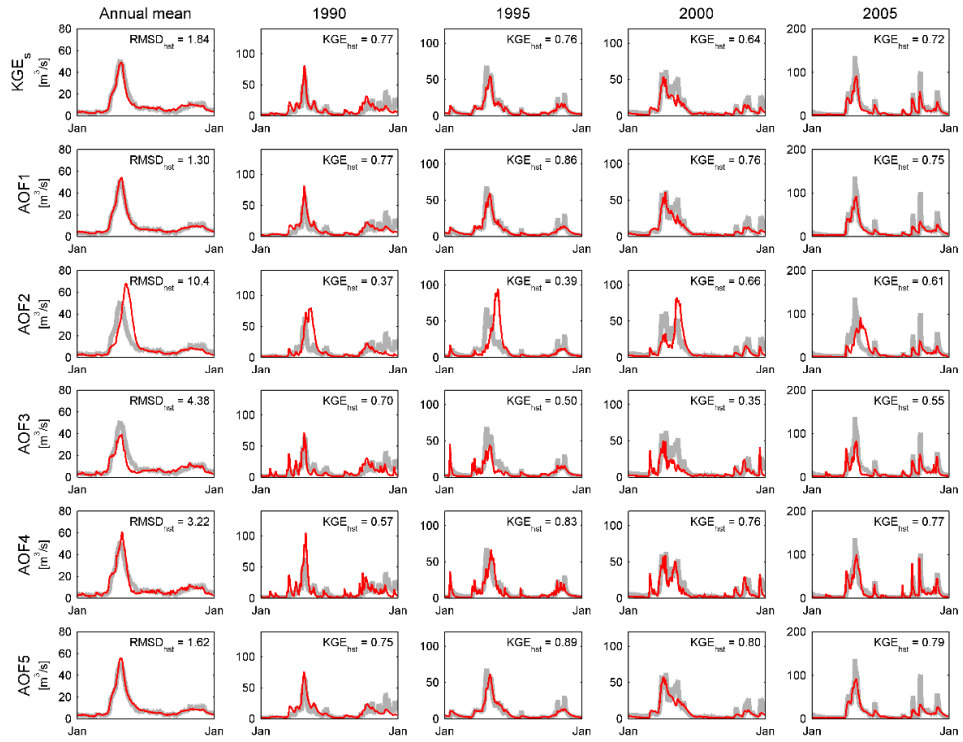

Figure 5. Observed (grey) and simulated (red) Du Loup River interannual and annual hydrographs (1990, 1995, 2000, and 2005, validation period). The WaSiM-ETH hydrologic model is forced and calibrated with historical meteorological observations (hst). Calibration is operated with a seasonal variation of the Kling-Gupta efficiency metric (KGE_s) and asynchronous objective functions *AOF1* to *AOF5*. Interannual performance is expressed in RMSD, annual performance, in KGE.

Figure 6 illustrates the distribution of the validation annual performance values for calibration exploiting the KGE_s or *AOF1* to *AOF5* for Du Loup, Nicolet Sud-Ouest and De l'Achigan catchments (Figure 3, sample size = 60, 20 years × 3 catchments). Performance is expressed in terms of KGE and its variance (α), bias (β), and correlation (*r)* components (Equation (13)). Hydrologic performance is presented separately for the nival (DJFMAM) and pluvial (JJASON) seasons. Nival KGE_s values range from 0.46 to 0.93: The median (M^{KGE,KGE_s}_{DJFMAM}) is 0.77. According to the non-parametric Wilcoxson rank-sum test, *AOF1* and *AOF5* offer nival performances comparable to the KGE*s* ($M^{KGE,AOF1}_{DJFMAM}$ = 0.73, p = 0.16, $M^{KGE,AOF5}_{DJFMAM}$ = 0.73, p = 0.21, significance level set to 0.05). *AOF4* do not lead to a comparable performance, the estimated p-value is however fairly close to the significance level ($M^{KGE,AOF4}_{DJFMAM}$ = 0.74, p = 0.02). The poor *AOF2* or *AOF3* representation of the nival flow regime, depicted in Figure 5, is here confirmed. Their median annual performance values are significantly degraded relative to KGE_s ($M^{KGE,AOF2}_{DJFMAM}$ = 0.56, $p = 2.59 \times 10^{-13}$ and $M^{KGE,AOF3}_{DJFMAM}$ = 0.55, $p = 1.13 \times 10^{-10}$). Poorer nival performances are driven by a severe degradation of the correlation (r), but also an overestimation of flow variance (α) for *AOF2*. Most AOFs (not *AOF3*) improve nival bias (β) over the KGE_s, while *AOF4* and *AOF5* improve flow variance. AOFs tend to degrade nival correlation relative to KGE_s, the degradation remains moderate for *AOF1* and *AOF5*, as for *AOF4* to a certain extent. Hydrologic performance over the pluvial season

(JJASON) is generally poorer than for the nival season (DJFMAM) due to a degradation in both variance and bias. Pluvial performance of the KGE_s ranges from −0.22 to 0.91 with $M_{JJASON}^{KGE,KGE_s} = 0.64$. Most AOFs (not *AOF2*) present moderate but significant degradation pluvial performances relative to KGE_s ($M_{JJASON}^{KGE,AOF1} = 0.53$, $p = 9.53 \times 10^{-5}$, $M_{JJASON}^{KGE,AOF2} = 0.37$, $p = 4.19 \times 10^{-6}$, $M_{JJASON}^{KGE,AOF3} = 0.57$, $p = 0.022$, $M_{JJASON}^{KGE,AOF4} = 0.56$, $p = 0.008$, $M_{JJASON}^{KGE,AOF5} = 0.55$, $p = 0.007$). The reduced AOF performance is driven by an underestimation of the flow variance (except for *AOF4*) and a degradation of the correlation. Most AOFs (not *AOF2*) improve however the pluvial bias representation (β) over the KGE_s.

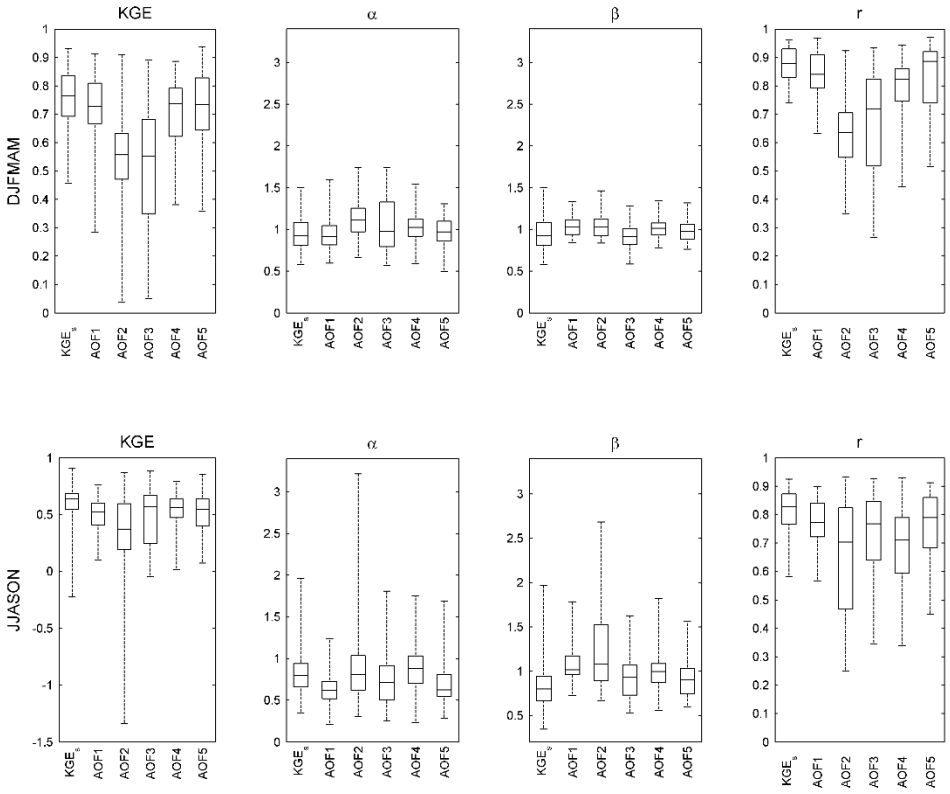

Figure 6. Hydrologic annual performance over the validation period for Du Loup, Nicolet Sud-Ouest and De l'Achigan catchments (n = 60). Calibration is operated with a seasonal variation of the Kling–Gupta efficiency (KGE_s) metric and asynchronous objective functions *AOF1* to *AOF5*. Performance is expressed in terms of KGE metric and its variance (α), bias (β), and correlation (r) components from December to May (DJFMAM) and June to November (JJASON).

3.2. Hydrologic Projections over the Reference Period

AOFs present site-specific hydrological responses over the historical period (see Appendix B). By and large however, most performing AOFs are considered to provide fairly comparable behaviors from one catchment to another and further analyses of the hydrologic projections conducted in this section are limited to *Du Loup* catchment (Figure 3). Figure 7 presents raw and corrected interannual air temperature and total precipitation taken from the first member of CRCM5-LE as well as the local observations. As denoted by Leduc et al. (2019) over Northeast America, a strong warm bias reaching +4 °C affects winter air temperature (Figure 7a). Another +2 °C bias is observed in summer. Applying quantile mapping (Section 2.3) narrows notably the seasonal biases, except for a residual ~+1°C bias in January. This residual winter bias affecting temperature can be explained by the coarse monthly sub-scaling of the transfers function combined to the length of the three-month moving window, which is potentially inappropriate for such large seasonal biases. Leduc et al. (2019) also denoted a +1 to +2 mm/day bias affecting CRCM5-LE simulated precipitation. The impact of bias correction on simulated total annual precipitation can be observed in Figure 7b. A residual negative bias up to −70 mm/a exists

for precipitation totals above 1000 mm/a. The latter can be explained by the scaling mismatch between simulated precipitation and interpolated data from in situ observation or the application of a fixed threshold correcting the drizzle effect [47]. Nonetheless, in both instances, quantile mapping largely improves the climate simulation over the reference period.

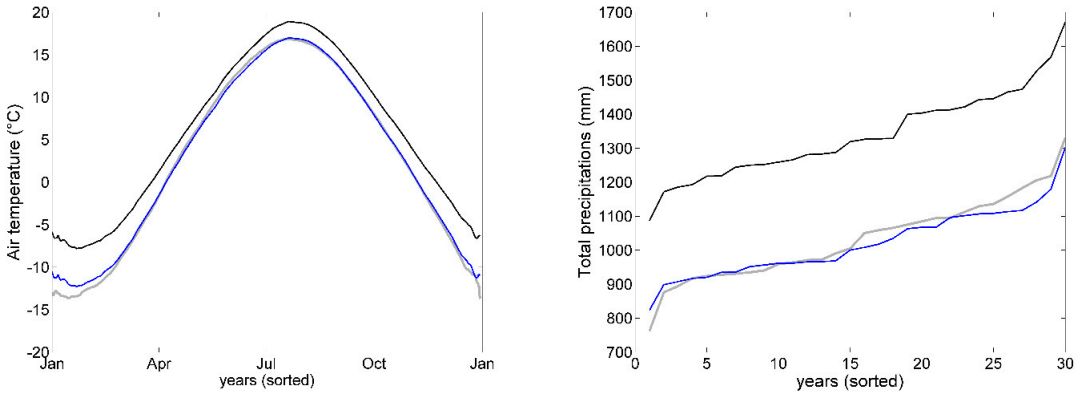

Figure 7. Observed (grey), raw (black), and bias-corrected (blue) interannual air temperature (**a**) and cumulative precipitations (**b**) simulated by the CRCM5-RCM over the Du Loup catchment.

Figure 8 compares the hydrologic projections simulated using both the conventional and alternative configurations of the hydroclimatic modeling chain (Figures 1 and 2), forced with bias-corrected air temperature and precipitation taken from the first member of the CRCM5-LE over the reference period (Figure 7). The WaSiM-ETH model is calibrated independently with KGE_s, *AOF1*, *AOF4*, and *AFO5* objective functions. *AOF2* and *AOF3* are excluded because their poor performance over the historical period (Section 3.1). Results are presented in Figure 8 as mean annual hydrographs and sorted logarithmic streamflow values below 10th and above 90th percentiles. Hydrologic projections are illustrated for both nival (DJFMAM) and pluvial (JJASON) seasons.

In all cases, projected mean annual hydrographs are affected by a notable degradation when compare to the performance achieved over the historical period ($RMSD_{hst}$ ranges from 1.30 m^3/s to 1.84 m^3/s, Figure 8). The amplitude of the projected nival flows is generally underestimated and out of phase. Within the conventional configuration (cnv), KGE_s offers a weak representation of the mean interannual hydrograph ($RMSD_{cvn,KGEs}$ = 5.60 m^3/s). It also offers a systematic underestimation of peak flows combined to an overestimation of low flow, regardless the season. Mean annual hydrographs simulated with the alternative configuration (alt) are systematically better than for the conventional configuration. Integrating AOFs, $RMSD_{alt}$ ranges from 3.74 m^3/s to 4.46 m^3/s. The latter enhances the amplitude and timing of the projected nival mean flows, which translate into an average improvement in terms of *RMSD* of 1.54 m^3/s relative to KGE_s within the conventional configuration.

The alternative configuration of the hydroclimatic modeling chain generally improves the representation of seasonal extremes values relative to KGE_s. *AOF5* provides the best representations of the projected nival peak flows ($RMSD_{alt,AOF5}$ = 0.03), while *AOF1* and *AOF4* underestimate and overestimate the latter respectively ($RMSD_{alt,AOF1}$ = 0.07, $RMSD_{alt,AOF4}$ = 0.08). The representation of extreme nival low flows is more accurate using *AOF4* and *AOF5* ($RMSD_{alt,AOF4}$ = 0.10, $RMSD_{alt,AOF5}$ = 0.09), but notably overestimated using *AOF1* ($RMSD_{alt,AOF1}$ = 0.57). Projected pluvial high flows are systematically underestimated. *AOF4* provides however a better representation than *AOF1* and *AOF5* ($RMSD_{alt,AOF4}$ = 0.22, $RMSD_{alt,AOF1}$ = 0.47, $RMSD_{alt,AOF5}$ = 0.43). On the other hand, projected pluvial low flows are generally overestimated: *AOF4* and *AOF5* ($RMSD_{alt,AOF4}$ = 0.21, $RMSD_{alt,AOF5}$ = 0.10) providing a better representation than *AOF1* ($RMSD_{alt,AOF1}$ = 0.49). Within the alternative configuration, KGE_s provides a surprisingly accurate representation of the mean annual hydrograph ($RMSD_{alt,KGEs}$ = 4.42 m^3/s) but fail to translate into a good representation of seasonal extreme values.

Projected nival low flows and high flows and pluvial low flows are notably degraded relative to the conventional configuration.

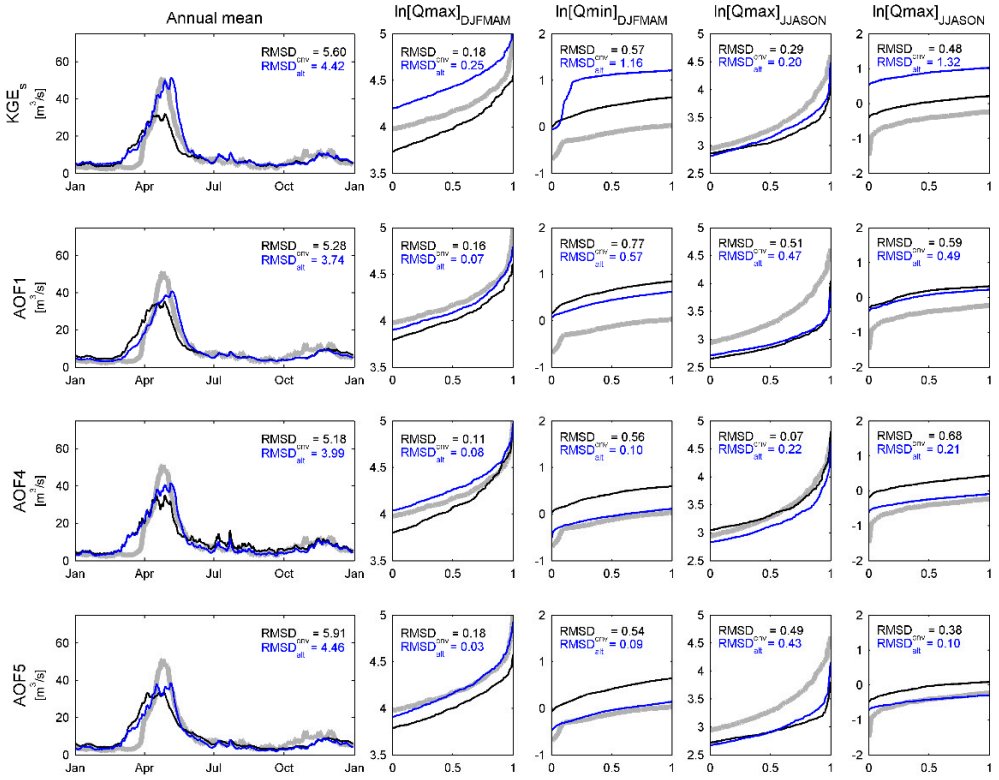

Figure 8. Observed (grey) and projected interannual hydrographs simulated by conventional (cvn, black) and alternative (alt, blue) configurations of the hydroclimatic modeling chain. The WaSiM-ETH hydrologic model is calibrated independently with KGE_s, *AOF1*, *AOF4*, and *AOF5* objective functions. Projections are also expressed through mean annual hydrographs and sorted logarithmic (ln) streamflow values below 10th and above 90th percentiles for both nival (DJFMAM) and pluvial (JJASON) seasons.

4. Discussion

4.1. AOFs *Provide an Appropriate Hydrological Response over the Historical Period*

Five exploratory asynchronous objective functions (AOFs) were designed and defined in Section 2.1 and used as calibration criteria purposely ignoring the correlation between simulated and observed streamflow. This property makes AOFs particularly suitable in a context where synchronicity between climate and hydrologic variables is unavailable; as in the case of constructing hydrologic projections using hydroclimatic modeling chains. Hydrologic performance of AOFs over the historical period was evaluated and compared to a seasonal variation of the Kling–Gupta efficiency metric (KGE). Results presented in Section 3.1 revealed the capacity of most performing AOFs to provide a hydrologic response comparable to KGE during the nival season, the latter being moderately degraded during the pluvial season. Hydrologic performance of AOFs is highly conditional to the application of a calibration criteria constraining an accurate representation of the interannual hydrologic cycle. AOFs excluding such a seasonal constrain (*AOF2* and *AOF3*) led to deficient representations of the flow regime. AOFs tend to reduce biases over both nival and pluvial seasons relative to KGE. Most performing AOFs also demonstrated a certain capacity to preserve the correlation, suggesting that the latter can be surrogated during the nival season by an appropriate interannual criteria within an AOF. AOFs tend to underestimate pluvial flow variance relative to KGE_s except for *AOF4* that fairs better. *AOF3* finally provided a hydrological response comparable to other performing AOFs in a strictly pluvial regime.

4.2. The Alternative Configuration of the Modeling Chain Enforces the Consistency of Hydrological Projections

An alternative configuration of the hydroclimatic modeling chain was tested and compared to a conventional configuration in Section 3.2. The WaSiM-ETH hydrologic model has been forced over the Du Loup catchment with bias corrected climate variables taken from CRCM5-LE over the reference period, instead of historical meteorological observations. Both conventional and alternative configurations were constructed independently with KGE_s and the best performing AOFs identified in Section 3.1 (*AOF1*, *AOF4*, and *AOF5*). The alternative configuration of the hydroclimatic modeling chain generally provided more coherent hydrologic projections relative to the conventional configuration. Projection of the interannual hydrograph was systematically improved, while seasonal extremes values were improved in most cases. The projected hydrologic response varied from one AOF to another. *AOF1* provided accurate projections of the mean annual hydrograph and nival peak flows. On the other hand, it underestimated pluvial peak flows and overestimated low flows, both nival and pluvial. The first order nature of *AOF1* (*RMSD* applied to interannual values) could explain its propensity to favor a sound representation of nival high flows to the expense of other hydrologic processes. In contrast, *AOF5* presented the most degraded projection of the interannual hydrograph, but the most performant projections of seasonal extremes values. Relative to *AOF1*, the construction by quantiles of *AOF5* weighted more effectively the extreme events. The absence of temporal sub-scaling within *AOF5* construction could explain the resulting degradation of the projected interannual hydrograph. Regardless a poorer performance over the historical period, *AOF4* presented a balanced projected hydrological response. Relative to other AOFs, *AOF4* did not notably degrade either the projected interannual hydrograph or seasonal extremes. Consequently, the application of a given AOF should be motived by the objectives defined in the scope of a given study. *AOF1* would be recommendable for assessment on water availability, *AOF5* for assessments on extremes, and *AOF4* for ecosystemic studies integrating multiple hydrologic considerations. Projections of the interannual hydrograph were affected by a systematic degradation relative to the historical period. This loss can be explained by a sensitivity of the hydrologic model to residual biases or inconsistency within post-processed climate variables. It can also be explained by a statistical mismatch between observed and simulated climate variable over the calibration period due to non-stationarity. Exploring a larger parametric space (Table 2) could have potentially provided better projected hydrological response, but would have further exposed the latter to overfitting.

4.3. Limitations

The work described in this manuscript is limited to many "singles": Single regional climate model, single member, single hydrologic model, single calibration period, etc. Generalising the applicably of AOFs within alternative configurations of the hydroclimatic modeling chain appears mandatory in further works. Applying the alternative configuration to a regional scale or large multi-members climate ensemble appears noteworthy challenges. Assessing the representability between calibration and validation periods considering non-stationary conditions between observations and multi-member climate simulations is another relevant question to further explore. Assessing the representability of the modelled sequence of extreme events prior to assessing formal statistical evaluation between the future and reference also appear relevant. Peaks-over-threshold statistical assessment could theoretically be very sensitive to a mismatch between the observed and modelled amount of extreme events over a given period. Other AOF constructions could also be tested. The intention while designing AOFs was to understand better their nature and behavior. More complex or performing AOFs can undoubtedly be designed, integrating additional *n*-moments, quantiles, or temporal sub-scaling. If available, other hydrological variables such as evapotranspiration, snow cover, or soil water content could be optimised in a similar way to *AOF1*. Variables simulated by a hydrologic model forced with historical meteorological observation could also surrogate observations. More complex constructions of AOFs would however further expose optimisation to equifinality and would thus request either an additional computing budget or adapted calibration strategies.

5. Conclusions

We introduced and tested an alternative configuration to the common hydroclimatic modeling chain with the aim of reinforcing the consistency of hydrological projections and circumventing the redundant usage of climate observations. We introduced a new type of calibration criteria, namely asynchronous objective functions (AOFs), which purposely ignore correlation between observed and simulated variables. The suggested configuration forces the hydrologic model with bias-corrected climate variables, thus preserving the sequence of events imbedded within the climate models. Results demonstrated that performing AOFs provided a hydrologic response comparable to the KGE metric over the nival historical period. They also demonstrated the capacity of the alternative configuration of hydroclimatic modeling chain to enforce the consistency of the projected interannual hydrograph and seasonal extreme values relative to a conventional configuration. AOFs presented distinct, but complementary, hydrologic responses, advocating for an appropriate application of AOFs according to the objective of a given study. The work described in this manuscript remains a proof of concept that requests further investigation and generalization to larger climate simulation ensembles, additional validation sites, and other climate regimes. This suggests, however, an innovative and fairly simple method enforcing the confidence affecting the production of hydrological projections.

Author Contributions: Conceptualization: S.R. and F.A.; methodology: S.R., J.-D.S., and F.A.; software: S.R.; validation: J.D.S. and F.A.; formal analysis: S.R.; investigation: S.R.; resources: J.-D.S. and F.A.; data curation: S.R.; writing—original draft preparation: S.R.; writing—review and editing: J.-D.S. and F.A.; visualization: S.R.; supervision: F.A.; project administration: J.-D.S. and F.A.; funding acquisition: J.-D.S., S.R., and F.A.

Funding: This research was funded by the Mitacs Accelerate program for scholarship to S.R. The authors wish to acknowledge the contributions of Ouranos and the Québec Ministry of Forests, Wildlife and Parks (MFFP project #142332118).

Acknowledgments: The authors also wish to acknowledge Quebec Ministry of Environment and Fight Against Climate Change (MELCC) for interpolated meteorological data (precipitation and temperature), hydrometric data, digital representation of the river network and integrated description of land uses.

Conflicts of Interest: The authors declare no conflict of interest.

Appendix A. Methodological Framework

Step 1. Testing AOFs

- Five exploratory AOFs are designed (*AOF1–AOF5*).
- The hydrologic model is forced with climate observations over three sites.
- Optimization is conducted with AOFs and KGE as cost-functions.
- Performance is evaluated between synchronized observed and simulated streamflow values using the KGE metric.
- AOFs presenting inappropriate performance are excluded from step 2.
- Site-to-site variability of the resulting simulated hydrological response is evaluated before conducting step 2 to one site.

Step 2. Comparing conventional and alternative configuration of the hydroclimatic modeling chain

- Conventional and alternative configurations of the hydroclimatic modeling chain are implemented. The hydrologic model is forced with climate simulation.
- Optimization is conducted with KGE and most performing AOFs as cost functions.
- Performance of both configurations is evaluated between asynchronized observed and projected streamflow values using metrics excluding correlation.

Appendix B. Site-to-Site Variability of the Simulated Hydrological Response

Figures A1–A3 present the distribution of the validation annual performance for Du Loup, Nicolet Sud-Ouest and De l'Achigan catchments evaluated independently (equivalent to Figure 6).

AOFs present site-specific hydrological responses over the historical period. While *AOF1* and *AOF5* outperform other AOFs over Du Loup catchment (Figure A1), AOFs offer a much more volatile response over Nicolet Sud-Ouest during the pluvial season (Figure A2). Long tailed distributions observed over De l'Achigan (Figure A3) are finally affected by isolated outlying weak annual performance values.

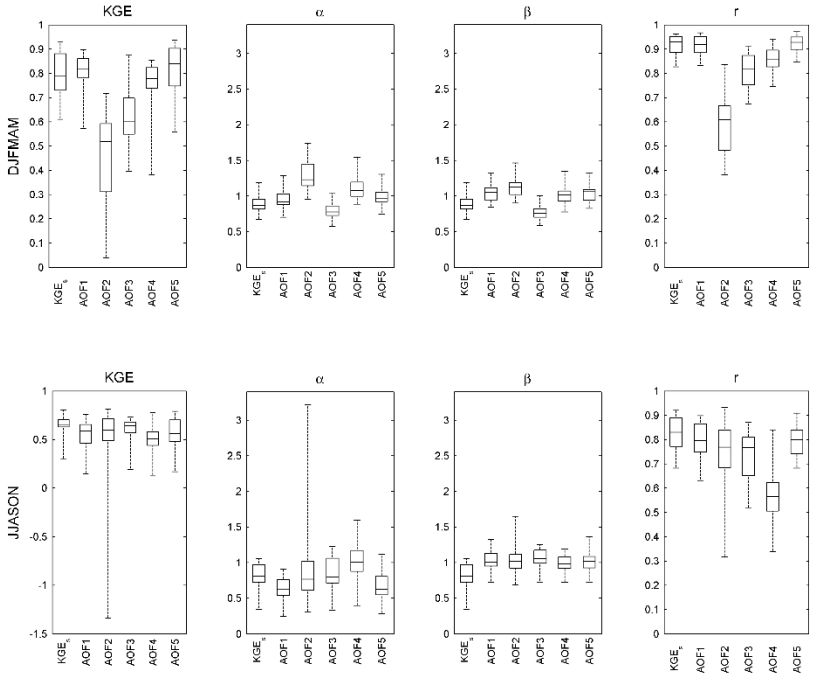

Figure A1. Hydrologic annual performance over the validation period for the Du Loup catchment (see Figure 6 for further description).

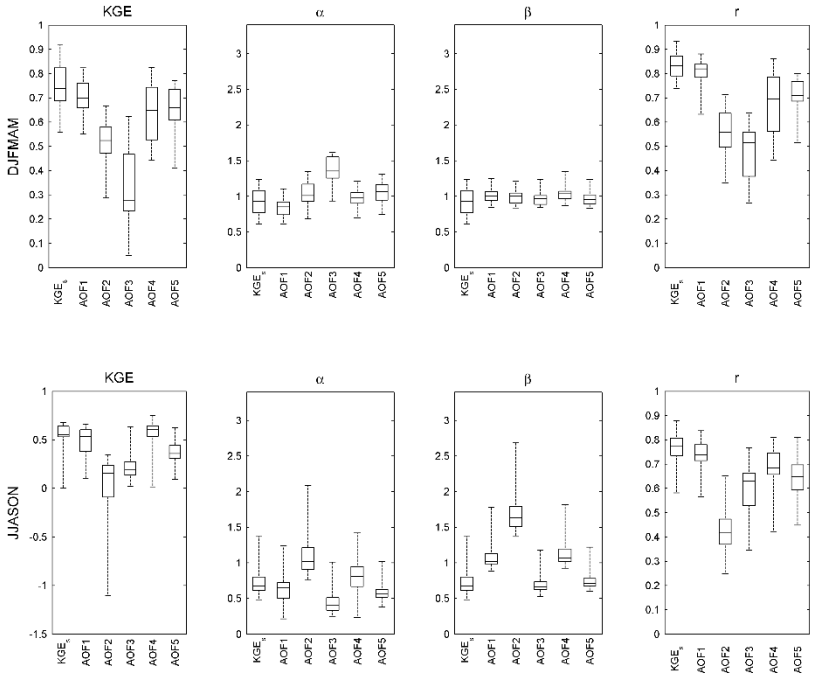

Figure A2. Hydrologic annual performance over the validation period for the Nicolet Sud-Ouest catchment (see Figure 6 for further description).

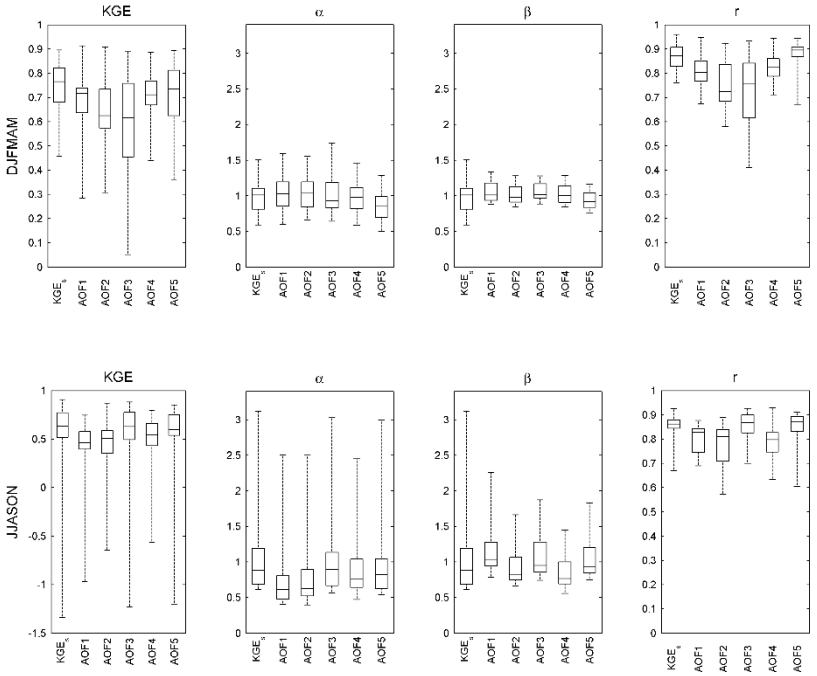

Figure A3. Hydrologic annual performance over the validation period for the De l'Achigan catchment (see Figure 6 for further description).

References

1. Madsen, H.; Lawrence, D.; Lang, M.; Martinkova, M.; Kjeldsen, T.R. Review of trend analysis and climate change projections of extreme precipitation and floods in Europe. *J. Hydrol.* **2014**, *519*, 3634–3650. [CrossRef]
2. Foughali, A.; Tramblay, Y.; Bargaoui, Z.; Carreau, J.; Ruelland, D. Hydrologic modeling in northern Tunisia with regional climate model outputs: Performance evaluation and bias-correction in present climate conditions. *Climate* **2015**, *3*, 459–473. [CrossRef]
3. Seong, C.; Sridhar, V. Hydroclimatic variability and change in the Chesapeake Bay watershed. *J. Water Clim. Chang.* **2017**, *8*, 254–273. [CrossRef]
4. Bozkurt, D.; Rojas, M.; Boisier, J.P.; Valdivieso, J. Projected hydroclimate changes over Andean basins in central Chile from downscaled CMIP5 models under the low and high emission scenarios. *Clim. Chang.* **2018**, *150*, 131–147. [CrossRef]
5. Giménez, P.O.; García-Galiano, S.G.; Giraldo-Osorio, J.D. Improvement of hydroclimatic projections over southeast Spain by applying a novel RCM ensemble approach. *Water* **2018**, *10*, 52.
6. Olsson, J.; Arheimer, B.; Borris, M.; Donnelly, C.; Foster, K.; Nikulin, G.; Persson, M.; Perttu, A.M.; Uvo, C.B.; Viklander, M.; et al. Hydrological Climate Change Impact Assessment at Small and Large Scales: Key Messages from Recent Progress in Sweden. *Climate* **2016**, *4*, 39. [CrossRef]
7. Themeßl, M.J.; Gobiet, A.; Leuprecht, A. Empirical-statistical downscaling and error correction of daily precipitation from regional climate models. *Int. J. Climatol.* **2011**, *31*, 1530–1544. [CrossRef]
8. Mpelasoka, F.S.; Chiew, F.H. Influence of Rainfall Scenario Construction Methods on Runoff Projections. *J. Hydrometeorol.* **2009**, *10*, 1168–1183. [CrossRef]
9. Zhang, L.; Su, F.; Yang, D.; Hao, D.; Tong, K. Discharge regime and simulation for the upstream of major rivers over Tibetan Plateau. *J. Geophys. Res. Atmos.* **2013**, *118*, 8500–8518. [CrossRef]
10. Higley, M.C.; Conroy, J.L. The hydrological response of surface water to recent climate variability: A remote sensing case study from the central tropical Pacific. *Hydrol. Process.* **2019**, *33*, 2227–2239. [CrossRef]
11. Uprety, M.; Ochoa-Tocachi, B.F.; Paula, J.D.; Regmid, S.; Buytaert, W. Improving water resources management using participatory monitoring in a remote mountainous region of Nepal. *J. Hydrol. Reg. Stud.* **2019**, *23*, 1–13. [CrossRef]

12. Essou, G.R.C.; Sabarly, F.; Lucas-Picher, P.; Brissette, F.; Poulin, A. Can precipitation and temperature from meteorological reanalyses be used for hydrological modeling? *J. Hydrometeorol.* **2016**, *17*, 1929–1950. [CrossRef]
13. Ricard, S.; Anctil, F. Forcing the Penman-Montheith Formulation with Humidity, Radiation, and Wind Speed Taken from Reanalyses, for Hydrologic Modeling. *Water* **2019**, *11*, 1214. [CrossRef]
14. Singh, H.; Sankarasubramanian, A. Systematic uncertainty reduction strategies for developing streamflow forecasts utilizing multiple climate models and hydrologic models. *Water Resour. Res.* **2014**, *50*, 1288–1307. [CrossRef]
15. Seo, S.B.; Sinha, T.; Mahinthakumar, G.; Sankarasubramanian, A.; Kumar, M. Identification of dominant source of errors in developing streamflow and groundwater projections under near-term climate change. *J. Geophys. Res. Atmos.* **2016**, *121*, 7652–7672. [CrossRef]
16. Climate Change in Australia. Available online: https://www.climatechangeinaustralia.gov.au/en/climate-campus/modelling-and-projections/climate-models/theory-and-physics/ (accessed on 10 September 2019).
17. Cannon, A.J. Multivariate quantile mapping bias correction: An N-dimensional probability density function transform for climate model simulations of multiple variables. *Clim. Dyn.* **2018**, *50*, 31–49. [CrossRef]
18. Piani, C.; Haerter, J.O.; Coppola, E. Statistical bias correction for daily precipitation in regional climate models over Europe. *Theor. Appl. Climatol.* **2010**, *99*, 187–192. [CrossRef]
19. Krysanova, V.; Donnelly, C.; Gelfan, A.; Gerten, D.; Arheimer, B.; Hattermann, F.; Kundzewicz, Z.W. How the performance of hydrologic models relates to credibility of projections under climate change. *Hydrol. Sci. J.* **2018**, *63*, 696–720. [CrossRef]
20. García, L.E.; Matthews, J.H.; Rodriguez, D.J.; Wijnen, M.; DiFrancesco, K.N.; Ray, P. *Beyond Downscaling: A Bottom-Up Approach to Climate Adaptation for Water Resources Management*; AGWA Report 01; World Bank Group: Washington, DC, USA, 2014; pp. 1–51.
21. Kay, A.L.; Crooks, S.M.; Reynard, N.S. Using response surfaces to estimate impacts of climate change on flood peaks: Assessment of uncertainty. *Hydrol. Process.* **2014**, *28*, 5273–5287. [CrossRef]
22. Guo, D.; Westra, S.; Maier, H.R. An inverse approach to perturb historical rainfall data for scenario-neutral climate impact studies. *J. Hydrol.* **2018**, *556*, 877–890. [CrossRef]
23. Ekström, M.; Gutmann, E.D.; Wilby, R.L.; Tye, M.R.; Kirono, D.G.C. Robustness of hydroclimate metrics for climate change impact research. *Water* **2018**, *5*, 1–20. [CrossRef]
24. Zhang, Y.; Shao, Q.; Zhang, S.; Zhai, X.; She, D. Multi-metric calibration of hydrological model to capture overall flow regimes. *J. Hydrol.* **2016**, *539*, 525–538. [CrossRef]
25. Pechlivanidis, I.G.; Jackson, B.; McMillan, H.; Gupta, H. Use of an entropy-based metric in multiobjective calibration to improve model performance. *Water Resour. Res.* **2014**, *50*, 8066–8083. [CrossRef]
26. Asadzadeh, M.; Tolson, B.A.; Burn, D.H. A new selection metric for multiobjective hydrologic model calibration. *Water Resour. Res.* **2014**, *50*, 7082–7099. [CrossRef]
27. Seiller, G.; Roy, R.; Anctil, F. Influence of three common calibration metrics on the diagnosis of climate change impacts on water resources. *J. Hydrol.* **2017**, *547*, 280–295. [CrossRef]
28. Mizukami, N.; Rakovec, O.; Newman, A.J.; Clark, M.P.; Wood, A.W.; Gupta, H.V.; Kumar, R. On the choice of calibration metrics for "high-flow" estimation using hydrologic models. *Hydrol. Earth Syst. Sci.* **2019**, *23*, 2601–2614. [CrossRef]
29. Cu, P.T.; Ball, J.E. The influence of the calibration metric on design flood estimation using continuous simulation. *Int. J. River Basin Manag.* **2017**, *15*, 9–20. [CrossRef]
30. Vansteenkiste, T.; Tavakoli, M.; Ntegeka, V.; De Smedt, F.; Batelaan, O.; Pereira, F.; Willems, P. Intercomparison of hydrological model structures and calibration approaches in climate scenario impact projections. *J. Hydrol.* **2014**, *519*, 743–755. [CrossRef]
31. Mendoza, P.A.; Clark, M.P.; Mizukami, N.; Gutmann, E.D.; Arnold, J.R.; Brekke, L.D.; Rajagopalan, B. How do hydrologic modeling decisions affect the portrayal of climate change impacts? *Hydrol. Process.* **2016**, *30*, 1071–1095. [CrossRef]
32. Barnston, A.G. Correspondence among the correlation, RMSE, and Heidke forecast verification measures. *Weather Forecast.* **1992**, *7*, 699–709. [CrossRef]
33. Nash, J.E.; Sutcliffe, J.V. River flow forecasting through conceptual models part I—A discussion of principles. *J. Hydrol.* **1970**, *10*, 282–290. [CrossRef]

34. Gupta, H.V.; Kling, H.; Yilmaz, K.K.; Martinez, G.F. Decomposition of the mean squared error and NSE performance criteria: Implications for improving hydrologic modelling. *J. Hydrol.* **2009**, *377*, 80–91. [CrossRef]
35. Chen, J.; Brissette, F.P.; Chaumont, D.; Braun, M. Finding appropriate bias correction methods in downscaling precipitation for hydrologic impact studies over North America. *Water Resour. Res.* **2013**, *49*, 4187–4205. [CrossRef]
36. WaSiM-ETH Documentation. Available online: http://www.wasim.ch/en/products/wasim_description.htm (accessed on 10 September 2019).
37. Vrzel, J.; Ludwig, R.; Gampe, D.; Ogrinc, N. Hydrologic system behaviour of an alluvial aquifer under climate change. *Sci. Total Environ.* **2019**, *649*, 1179–1188. [CrossRef]
38. Shangguan, W.; Dai, Y.; Duan, Q.; Liu, B.; Yuan, H. A global soil data set for earth system modeling. *J. Adv. Model. Earth Syst.* **2014**, *6*, 249–263. [CrossRef]
39. Federer, C.A.; Lash, D. *BROOK—A Hydrologic Simulation Model for Eastern Forests*; Research Report No. 19; Water Resources Research Center: Durham, NC, USA, 1978.
40. Richards, L.A. Capillary conduction of liquids through porous mediums. *Physics* **1931**, *1*, 318–333. [CrossRef]
41. Van Genuchten, M.T. A Closed-Form Equation for Predicting the Hydraulic Conductivity of Unsaturated Soils. *Soil Sci. Soc. Am. J.* **1976**, *44*, 892–898. [CrossRef]
42. Asadzadeh, M.; Tolson, B. Hybrid Pareto archived dynamically dimensioned search for multi-objective combinatorial optimization: Application to water distribution network design. *J. Hydroinform.* **2012**, *14*, 192–205. [CrossRef]
43. Leduc, M.; Mailhot, A.; Frigon, A.; Martel, J.L.; Ludwig, R.; Brietzke, G.B.; Giguère, M.; Brissette, F.; Turcotte, R.; Braun, M.; et al. The ClimEx Project: A 50-Member Ensemble of Climate Change Projections at 12-km Resolution over Europe and Northeastern North America with the Canadian Regional Climate Model (CRCM5). *J. Appl. Meteorol. Clim.* **2019**, *58*, 663–693. [CrossRef]
44. Kirchmeier-Young, M.C.; Zwiers, F.W.; Gillett, N.P. Attribution of extreme events in Arctic Sea ice extent. *J. Clim.* **2017**, *30*, 553–571. [CrossRef]
45. Šeparovic, L.; Alexandru, A.; Laprise, R.; Martynov, A.; Sushama, L.; Winger, K.; Tete, K.; Valin, M. Present climate and climate change over North America as simulated by the fifth-generation Canadian regional climate model. *Clim. Dyn.* **2013**, *41*, 3167–3201. [CrossRef]
46. Ivanov, M.A.; Kotlarski, S. Assessing distribution-based climate model bias correction methods over an alpine domain: Added value and limitations. *Int. J. Climatol.* **2017**, *37*, 2633–2653. [CrossRef]
47. Schmidli, J.; Frei, C.; Vidale, P.L. Downscaling from GCM precipitation: A benchmark for dynamical and statistical downscaling methods. *Int. J. Climatol.* **2006**, *26*, 679–689. [CrossRef]

Section D : Informations complémentaires

4.1 Progrès lié au processus de réalisation du projet

i) Sommaire des étapes

1. Mise en place du modèle hydrologique WaSiM-ETH sur un ensemble de bassins versants forestiers du Québec.
2. Formatage des champs météorologiques observés (précipitations et température).
3. Formatage des champs simulées par des réanalyses (humidité relative, rayonnement solaire et vitesse du vent).
4. Formatage des simulations de l'ensemble climatique CRCM5-LE.
5. Mise en place de l'optimisateur PA-DDS et adaptation pour l'optimisation des fonctions de transfert.
6. Conception et évaluation des fonctions objectifs-asynchrones.
7. Production des projections hydrologiques.
8. Analyse des résultats.

i) Sommaire des livrables

1. Modèle hydrologique WaSiM-ETH et optimisateur PA-DDS opérationnel sur un ensemble de bassins versants forestiers du Québec.
2. Réponse hydrologique simulée sur la période historique à partir des formulations de Hamon et de Penman-Monteith sur un ensemble de bassins versants forestiers du Québec.
3. Projections hydroclimatiques simulées sur le bassin versant de la rivière Du Loup à partir de la formulation de Penman-Montheith et de l'ensemble climatique CRCM5-LE.
4. Deux publications scientifiques revues par les pairs, un rapport d'étape, un rapport final et présentation des résultats (séminaire Ouranos prévue le 10 février 2020).

*Le tableau ci-dessous résume les livrables déjà disponibles chez Ouranos. Veuillez le compléter et transmettre **par courriel** les livrables manquants ou qui ont été mis à jour depuis le dernier rapport d'étape.*

Publications, exposés et rapports				
Type de document ***Titre, année de publication, liste des auteurs, nom de la revue ou de l'organisme ou du congrès***	***Prévu ou soumis (date)***	***Accepté / Publié (date)***	***Présenté (date)***	***Nb de participant***
Articles dans une publication avec comité de lecture				
Forcing the Penman-Montheith Formulation with Humidity, Radiation, andWind Speed Taken from Reanalyses, for Hydrologic Modeling. doi:10.3390/w11061214		Publié (11 juin 2019)		

Exploring an Alternative Configuration of the Hydroclimatic Modeling Chain, Based on the Notion of Asynchronous Objective Functions. doi:10.3390/w11102012		Publié (27 septembre 2019)		
Optimizing quantile mapping transfer-functions for construction of physically-based streamflow projection in a context of observation scarcity.	Soumission prevue pour février 2020.			
Exposés à l'occasion de conférence ou affiches				
Exposé 1 / affiche 1				
Exposés ou rapports aux partenaires ou usagers				
Séminaire Ouranos			Prévu (10 février 2020).	
Autres (incluant les rapports techniques, les articles sans comité de lecture, les feuillets techniques, sites internet etc.)				
Rapport d'étape	Soumis (8 avril 2019)			

ii) Leçons apprises

Généraliser les retombées du projet à de plus larges ensembles climatiques.

iii) Obstacles et solutions

Le projet s'est généralement bien déroulé. Les objectifs définis dans la proposition initiale étaient modestes. La réalisation du projet s'est donc déroulée sans obstacles majeurs. Seule l'évaluation de l'impact de l'échantillonnage des membres climatiques sur la réponse hydrologique simulée a été abandonnée en cours de réalisation. Cette question n'a pas été jugée stratégique et prioritaire pour fins de publication.

iv) Retombées du projet

Le projet propose une configuration alternative de la chaîne de modélisation hydroclimatique ayant trois principales retombées potentielles sur la pratique en modélisation hydroclimatique :

1. *Accroître la confiance des projections hydroclimatiques en intégrant une représentation des processus hydrologiques davantage fondée sur une description physique des processus.*
2. *Produire des analyses d'impact pour des régions affectées par la rareté des observations météorologiques.*
3. *Projeter des variables hydrologiques intermédiaires davantage fondées sur une représentation physique des processus hydrologiques afin d'alimenter des modèles de croissance forestière.*

v) Futures activités

Des discussions seront tenues avec les partenaires sur une éventuelle suite au projet.

4.2 Aspects administratifs du projet

i) Réunions du comité de suivi

Dates des réunions du comité de suivi	*Compte-rendu transmis à Ouranos (oui/non)*
15 janvier 2019	Oui.
20 janvier 2020	Oui.

ii) Formation

Type de ressource	*(a) Université*	*(b) Date de début/de fin*	*(c) Nb d'heures par mois*	*(d) Nom du superviseur*
Assistant de recherche stagiaire				
Étudiant post-doc 1				
PhD 1	Université Laval	14 septembre 2018 au 20 janvier 2020	35	François Anctil
Étudiant maîtrise 1				
Étudiant bac 1				

iii)

iv) Contribution des partenaires

Nom des partenaires	*MITACS*	*Ouranos*	*MFFP-DRF*	
Le partenaire a contribué en espèces au projet	Oui	Oui	Oui	
Le partenaire a contribué en nature au projet	Oui	Oui	Oui	
Le partenaire était disponible aux fins de consultation		Oui	Oui	
Le partenaire a participé aux réunions du comité de suivi.		Oui	Oui	
Le partenaire a discuté sur une base régulière avec l'équipe universitaire.		Oui	Oui	
Si oui, indiquez le nombre de réunions tenues au cours de la période visée par le présent rapport		Oui, 5 réunions	Oui, 5 réunions	
Le partenaire a participé à la recherche (analyse, rédaction, organisation d'ateliers…).		Oui	Oui	
Autre type de participation (précisez)				

Contributions en espèces	*Montant total contribué à ce jour ($)*
MITACS	30 000
MFFP-DRF	25 000
Ouranos	5 000

Rappel : un rapport financier dûment signé doit également être soumis par le service des finances

Contributions en nature	*Nbre de représentants ayant participé au projet*	*Nbre total d'heures contribuées à ce jour par ces représentants*	*Nom de la personne contact*
MFFP-DRF	1	200	Jean-Daniel Sylvain
Ouranos	2	100	Diane Chaumont

v) Liste des usagers et bénéficiaires des résultats

Ministère des Forêts, de la Faune et des Parcs, Direction de la recherche forestière (MFFP-DRF).